

ACCEPTED MANUSCRIPT

Oximetry using multispectral imaging: theory and application

To cite this article before publication: Lewis E MacKenzie *et al* 2018 *J. Opt.* in press <https://doi.org/10.1088/2040-8986/aab74c>

Manuscript version: Accepted Manuscript

Accepted Manuscript is “the version of the article accepted for publication including all changes made as a result of the peer review process, and which may also include the addition to the article by IOP Publishing of a header, an article ID, a cover sheet and/or an ‘Accepted Manuscript’ watermark, but excluding any other editing, typesetting or other changes made by IOP Publishing and/or its licensors”

This Accepted Manuscript is © 2018 IOP Publishing Ltd.

During the embargo period (the 12 month period from the publication of the Version of Record of this article), the Accepted Manuscript is fully protected by copyright and cannot be reused or reposted elsewhere. As the Version of Record of this article is going to be / has been published on a subscription basis, this Accepted Manuscript is available for reuse under a CC BY-NC-ND 3.0 licence after the 12 month embargo period.

After the embargo period, everyone is permitted to use copy and redistribute this article for non-commercial purposes only, provided that they adhere to all the terms of the licence <https://creativecommons.org/licenses/by-nc-nd/3.0>

Although reasonable endeavours have been taken to obtain all necessary permissions from third parties to include their copyrighted content within this article, their full citation and copyright line may not be present in this Accepted Manuscript version. Before using any content from this article, please refer to the Version of Record on IOPscience once published for full citation and copyright details, as permissions will likely be required. All third party content is fully copyright protected, unless specifically stated otherwise in the figure caption in the Version of Record.

View the [article online](#) for updates and enhancements.

Oximetry using multispectral imaging: theory and application

Lewis E. MacKenzie¹, Andrew R Harvey²

1. Department of Chemistry, Faculty of Science, Durham University, Durham, UK. DL1 3LE.
2. School of Physics and Astronomy, College of Science and Engineering, University of Glasgow, UK. G12 8QQ.

E-mail: Lewis.E.MacKenzie@Durham.ac.uk

Abstract. Multispectral imaging (MSI) is widely applied across various imaging modalities as a technique for measurement of blood oxygen saturation (OS) *in vivo*, consequently providing new information about physiology and disease development. This tutorial aims to provide a thorough introduction to the theory and application of MSI oximetry for researchers new to the field, whilst also providing detailed information for more experienced researchers. The optical theory underlying two-wavelength oximetry, three-wavelength oximetry, pulse oximetry, and multispectral oximetry algorithms are described in detail. The varied challenges of applying MSI oximetry to *in vivo* applications are outlined and discussed, covering: the optical properties of blood and tissue, optical paths in blood vessels, tissue auto-fluorescence, oxygen diffusion, and common oximetry artefacts. Essential image processing techniques for MSI are discussed, in particular, image acquisition, image registration strategies, and blood vessel line profile fitting. Calibration and validation strategies for MSI are discussed, including comparison techniques, physiological interventions, and phantoms. The optical principles and unique imaging capabilities of various cutting-edge MSI oximetry techniques are discussed, including photoacoustic imaging, spectroscopic optical coherence tomography, and snapshot MSI.

1
2
3
4
5
6
7 **1 Contents**

8
9 **2 1. Introduction**

10
11 1.1 The application and utility of multispectral imaging oximetry ----- **3**
12 1.2 The principle of optical oximetry ----- **3**
13 1.3 Milestones in the development of MSI oximetry technology ----- **5**

14 **6 2. Theory of oximetry**

15 2.1 Two wavelength oximetry ----- **6**
16 2.2 Pulse oximetry ----- **9**
17 2.3 Three-wavelength oximetry ----- **10**
18 2.4 Multispectral oximetry ----- **11**

19 **10 3. Challenges for in vivo multispectral imaging oximetry**

20 3.1 Optical absorption by haemoglobin variants and blood plasma ----- **14**
21 3.2 Pigmentation in tissue ----- **15**
22 3.3 Optical scattering by tissue ----- **15**
23 3.4 Other challenges of imaging through tissue ----- **16**
24 3.5 Scattering by blood ----- **17**
25 3.6 Mitigating specular reflections from blood vessels ----- **18**
26 3.7 Optical paths through blood vessels ----- **19**
27 3.8 Rattlesnake artefacts ----- **20**
28 3.9 Oxygen diffusion ----- **20**
29 3.10 Multi-OS laminar flow in trunk veins ----- **22**

30 **21 4. Image processing for multispectral imaging oximetry**

31 4.1 Image acquisition ----- **22**
32 4.2 Co-registration of multispectral images ----- **23**
33 4.3 Estimating the Transmission of blood vessels ----- **25**

34 **26 5. Strategies for validation of multispectral imaging oximetry**

35 5.1 Testing fundamental optical assumptions: Monte Carlo simulations ----- **26**
36 5.2 Validation with artificial phantoms ----- **27**
37 5.3 In vivo validation strategies ----- **27**

38 **30 6. Multispectral oximetry imaging modalities**

39 6.1 Time-sequential multispectral imaging ----- **29**
40 6.2 Snapshot multispectral imaging oximetry ----- **29**
41 6.3 Scanning laser ophthalmoscopes ----- **30**
42 6.4 Photoacoustic imaging ----- **30**
43 6.5 Spectroscopic Optical Coherence Tomography ----- **31**
44 6.6 Dual-wavelength photothermal optical ----- **31**

45 **37 7. Summary and Conclusions ----- 31**

1. Introduction

1.1. The application and utility of multispectral imaging oximetry

Highly localized measurement of blood oxygen saturation (OS) within tissue is useful for establishing physiological norms, and for monitoring hyperoxia (i.e. elevated OS) and hypoxia (i.e. reduced OS); which can be cause or symptom of various diseases. For example, hyperoxia is associated with retinopathy of prematurity[1]; arterial occlusion induces hypoxia, with subsequent loss of tissue function[2]; and cancerous tumours can cause localized hypoxia due to excessive metabolic demand.[3,4] However, many commonly used oximetry techniques, including blood gas measurement and pulse oximetry, lack the spatial resolution or tissue specificity required to measure blood OS in a manner relevant for detail studies of physiology or disease development. Multispectral imaging (MSI) oximetry is an optical technique that utilises the OS-dependent absorption spectra of haemoglobin within blood to quantify OS with high spatial and temporal resolution. This makes MSI oximetry ideal for highly specific studies of OS in small blood vessels that supply tissue.[5]

MSI oximetry can be applied with various imaging techniques to image blood vessels in different bodily tissues. For example, MSI retinal fundus cameras are utilized for measuring blood oxygen in the eye[6], and MSI microscopes can be used to measure oxygen within individual red blood cells.[5] Emerging imaging modalities such as photoacoustic tomography (PAT) and spectroscopic optical coherence tomography (S-OCT) have also been utilized to provide enhanced oximetry imaging capabilities: PAT enables oximetry in deep tissue, and S-OCT provides simultaneous 3D mapping of both tissue and OS (see Section 6).

MSI oximetry has been applied to diverse applications *in vivo*, including measurement of blood OS in the spinal cord,[7] the brain,[8] muscle tendons,[9,10] the bowel,[11] the oral microvasculature,[12] and the skin.[13] In the eye, MSI oximetry has established the oxygen dynamics and physiological norms of the retina,[6] the choroid,[14] the bulbar conjunctiva,[15] and the episcleral blood vessels.[15]

Various diseases have been studied with MSI oximetry, including diabetic retinopathy,[16,17] glaucoma,[18–20] retinal vessel occlusion,[2,6] stroke,[8] rheumatoid arthritis,[10] diabetic foot ulcers,[13,21] and cancerous tumor development.[3,22] For the full applications of oximetry to the monitoring of retinal disease, readers are referred to recent reviews.[6,23,24]

1.2. The principle of optical oximetry

The theory of MSI oximetry is fundamentally the same across all imaging techniques, in that all MSI modalities measure the OS-dependent absorption of light by haemoglobin (see Figure 1). Haemoglobin is the dominant absorber of light in blood, with typically ~250 million haemoglobin molecules inside a normal red blood cell (RBC).[25] The function of haemoglobin is to transport oxygen around the body by reversible binding of oxygen to four heme sub-units. These heme units strongly absorb blue and green light, giving haemoglobin its distinctive red colour.* When oxygen binds or unbinds to haemoglobin, the optical absorbance properties of haemoglobin are altered, resulting in a change in the optical absorption spectra of blood (see Figure 1).† The affinity of haemoglobin for oxygen is described by the sigmoid-shaped oxygen dissociation curve, which varies with temperature and pH, as well as between species.[26] Each haemoglobin molecule can bind up to four oxygen molecules: one to each

* Note that contrary to popular belief, deoxygenated blood is not blue. The blue appearance of veins through skin tissue is due to the combination of multiple effects, including optical scattering and absorption by tissue, combined with quirks of human visual perception.[159]

† The change in optical absorbance of haemoglobin as oxygen binds or unbinds is due to a change in electron configuration of haemoglobin.

1 heme group – resulting in five possible states for each individual haemoglobin molecule: 0%, 25%,
 2 50%, 75%, and 100% oxygen occupancy. A population of many haemoglobin molecules can be of an
 3 average OS anywhere between 0 – 100% OS.

4 The OS of blood is defined as:

$$l p_{\text{O}_2} = \frac{C_{\text{O}_2\text{Hb}}}{C_{\text{HbT}}} = \frac{C_{\text{O}_2\text{Hb}}}{C_{\text{O}_2\text{Hb}} + C_{\text{Hb}}},$$

5 Where C_{HbT} , $C_{\text{O}_2\text{Hb}}$, and C_{Hb} are, respectively, the molar concentrations of total haemoglobin, fully
 6 oxygenated haemoglobin, and fully deoxygenated haemoglobin. For typical arteries (i.e. blood vessels
 7 carrying oxygenated blood away from the heart), nominal OS is in the range 94 - 98%, corresponding
 8 to a partial pressure of oxygen ($p\text{O}_2$) of ~ 100 mmHg. In typical veins (i.e. deoxygenated blood vessels
 9 carrying blood towards the heart), nominal OS is ~70%, corresponding to a $p\text{O}_2$ ~ 40 mmHg.[27]
 10 However, OS values within the body vary considerably, depending on parameters, such as the
 11 atmospheric partial pressure of oxygen ($p\text{O}_2$), blood flow velocity, and metabolic demand by tissue. For
 12 example, the metabolic demand for oxygen in retinal tissue is particularly high, resulting in venous OS
 13 ~60%.[28]

14 The absorption spectra of fully oxygenated haemoglobin (O_2Hb) and fully deoxygenated haemoglobin
 15 (Hb) are shown in Figure 1. The spectra exhibit several isobestic wavelengths, at which the extinction
 16 coefficients of haemoglobin are insensitive to changes in OS, interspersed with spectral bands where the
 17 extinction coefficients vary strongly with OS. Two-wavelength oximetry, a simple approach to
 18 oximetry, exploits the approximately linear relationship between OS and the ratio of measured optical-
 19 density at an isobestic waveband to the optical-density at an OS-sensitive waveband. The strength of
 20 such a ratiometric technique arises from the simplicity of application: however, the assumption of
 21 linearity, based on the Beer-Lambert law, is an over-simplification, where presence of optical scattering
 22 and additional chromophores in neighboring tissue, or indeed other species of Hb within the blood, can
 23 lead to inaccuracies.[29] The use of multispectral imaging with various degrees of sophistication and
 24 complexity provides scope for increased accuracy and robustness in oximetry. Simply put, recording the
 25 absorption of blood at more wavelengths enables more unknown parameters to be accounted for,
 26 improving oximetry (see Section 2.4).

27

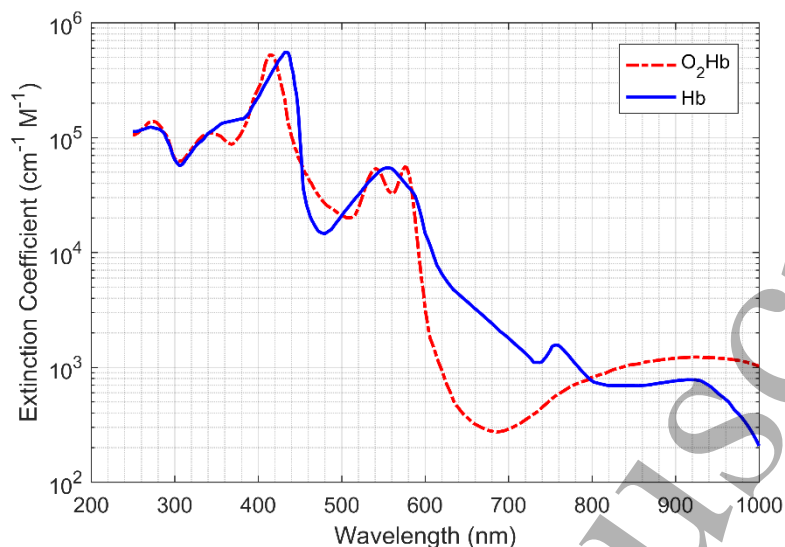


Figure 1. The optical absorption spectra of oxygenated haemoglobin (HbO₂) [the red line] and deoxygenated haemoglobin (Hb) [the blue line]. Figure created from spectroscopic data tabulated by S. Prahl (1999). [30] The units for extinction coefficient are per centimetre per mole (cm⁻¹ M⁻¹).

1.3. Milestones in the development of MSI oximetry technology

The pioneering MSI oximetry studies of retinal OS were undertaken in the 1960s, establishing the fundamental principles of two-wavelength oximetry upon which all subsequent research has been built. [31–33] Initially, retinal oximetry was calibrated by *ex vivo* blood gas measurement. However, the advent of fingertip pulse oximetry subsequently enabled simpler calibration by non-invasive measurement of arterial OS via the fingertip (see Section 2.2). [34] Later oximetry studies advanced the field by establishing techniques such as three-wavelength oximetry, [35] scanning laser retinal MSI, [36] and high spectral resolution retinal spectrophotometry. [37,38] For more detailed information on the development of retinal oximetry, the reader is referred to the 2014 retrospective by Jim Beach. [24]

In the late 1990s, digital imaging technology began to replace photographic cameras, paving the way for automated computational analysis of images. [24,39] The mid-to-late 2000s saw the development of two commercially available retinal oximetry systems; the Oxymap T1 retinal oximeter (Oxymap ehf, Iceland) [40] and the Imedos retinal oximeter (Imedos Systems UG, Germany). [17] Advances in computational power and techniques enabled automatic oximetry, consequently enabling the study of numerous retinal diseases by ophthalmologists. [23]

In the past decade, emerging imaging modalities have enabled MSI oximetry to be applied to increasingly diverse *in vivo* applications. Snapshot MSI systems have enabled oximetry with sub-second temporal resolution, enabling observations of fast biological processes such as oxygen diffusion into the microvasculature [15] and MSI endoscopes have provided measurements in tissue that are not accessible with traditional imaging techniques, e.g. within the bowel. [11] Photoacoustic techniques have enabled deep-tissue oximetry of the brain, cancer tumors, and entire small animals, [41] and spectroscopic optical coherence tomography (S-OCT) has enabled complimentary 3D mapping of OS and tissue structure. [42] Across all MSI modalities, advancement and application of MSI oximetry technology has yielded considerable insights into physiological norms and disease development. [6] Section 6 provides further details on the applications and optical principles underpinning these emerging MSI modalities.

2. Theory of oximetry

1 2.1. Two-wavelength oximetry

2 2.1.1. Derivation of two-wavelength oximetry

3 The simplest and most commonly used form of oximetry is two-wavelength oximetry, which is based
4 on the Beer-Lambert law of light transmission through a medium:

$$5 I_{\lambda} = I_{\lambda_0} \exp(-c \varepsilon_{\lambda} d) \quad 2$$

6 where I_{λ} is the intensity of the light transmitted through the medium, I_{λ_0} is the intensity of the light
7 incident upon blood, c is the molar concentration of absorbers (i.e. haemoglobin) within blood [M], ε_{λ}
8 is the wavelength-dependent molar extinction coefficient of haemoglobin [$\text{cm}^{-1}\text{M}^{-1}$], and d is the optical
9 path length of light through the blood [cm]. For blood, ε_{λ} is defined by:

$$10 \varepsilon_{\lambda} = (OS \varepsilon_{\lambda_{O_2Hb}} + (1-OS) \varepsilon_{\lambda_{Hb}}) \quad 3$$

11 where OS is the fractional blood oxygen saturation (range 0-1), $\varepsilon_{\lambda_{O_2Hb}}$ is the molar extinction
12 coefficient of fully oxygenated haemoglobin, and $\varepsilon_{\lambda_{Hb}}$ is the molar extinction coefficient of
13 deoxygenated haemoglobin. No other chromophores are included in this simplified model. The
14 transmission, T_{λ} , of the blood is defined as:

$$15 T_{\lambda} = \left(\frac{I_{\lambda}}{I_{\lambda_0}} \right) \quad 4$$

16 The optical-density (OD) of the blood at a given wavelength, OD_{λ} is then defined as:

$$17 OD_{\lambda} = -\log(T_{\lambda}) = c d \varepsilon_{\lambda} \quad 5$$

18 Assuming that c and d are identical at both wavelengths, then the optical-density ratio, ODR, is:

$$19 ODR = \frac{OD_{\lambda_1}}{OD_{\lambda_2}} = \frac{c d \varepsilon_{\lambda_1}}{c d \varepsilon_{\lambda_2}} = \frac{\varepsilon_{\lambda_1}}{\varepsilon_{\lambda_2}} \quad 6$$

20 If one wavelength is chosen to be isobestic, i.e. insensitive to changes in OS, and the other wavelength
21 is chosen to be sensitive to changes in OS, then ODR will be linearly proportional to OS.[31] If nominal
22 OS values are known by independent means, then ODR can be empirically calibrated to OS by fitting
23 ODR to the equation of a straight line, i.e.:

$$24 OS = a * ODR + b, \quad 7$$

25 where a and b are empirically derived calibration coefficients obtained by plotting ODR vs. OS. Thus,
26 from measuring transmission at two wavelengths, ODR can be calculated, from which OS can be
27 estimated by empirical calibration.

28 2.1.2. Optimal vessel transmission and wavelength combinations for two-wavelength oximetry

29 For accurate oximetry, blood vessels must neither be too transparent nor too opaque. Based upon work
30 by Assendelft (1970),[43] Smith derived the following optimal transmission for a blood vessel in order
31 to minimize sensitivity of OS to transmission measurement uncertainty/error.[44] Smith's derivation
32 starts from the definition of optical-density, OD_{λ} :

$$33 OD_{\lambda} = -\log(T_{\lambda}) = \frac{\ln(T_{\lambda})}{\ln(10)} \quad 8$$

34 The absolute error function for OD_{λ} is then found by differentiating:

$$35 \Delta OD_{\lambda} = \frac{dOD_{\lambda}}{dT_{\lambda}} \Delta T_{\lambda} = \frac{\Delta T_{\lambda}}{\ln(10) T_{\lambda}} \quad 9$$

36 The fractional error function of OD_{λ} is then:

$$\frac{\Delta OD_\lambda}{OD_\lambda} = \frac{\Delta T_\lambda}{T_\lambda \ln(T_\lambda)}. \quad 10$$

1 To minimise the relative error of OD_λ , the first derivative, with respect to T_λ , of Equation 10 must be
 2 found, and then set to zero.

$$\frac{d(\Delta OD_\lambda / OD_\lambda)}{dT_\lambda} = \frac{\ln(T_\lambda) + 1}{[T_\lambda \ln(T_\lambda)]^2} \Delta T_\lambda = 0. \quad 11$$

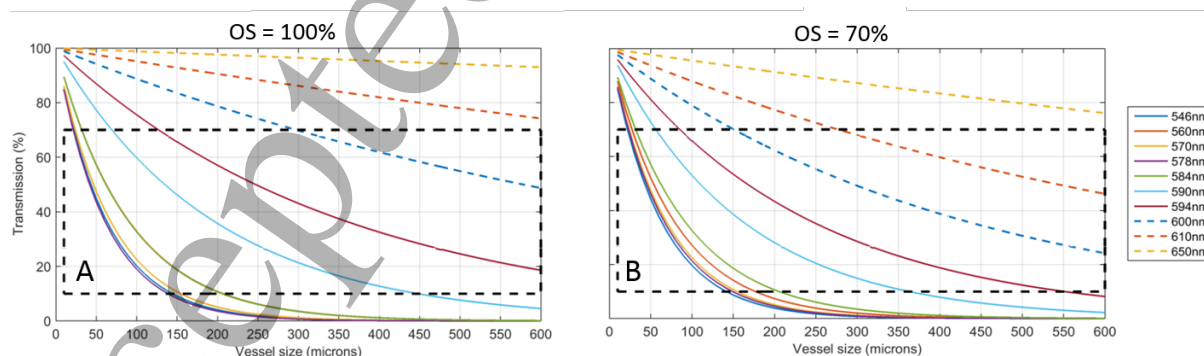
3 Discarding the non-physical solution of $T_\lambda = 0$, leaves the following solution:

$$\begin{aligned} \ln(T_\lambda) + 1 &= 0, \\ \Rightarrow T_\lambda &= 1/e = 36.8\%, \\ \Rightarrow OD_\lambda &= 0.434. \end{aligned} \quad 12$$

4 This solution indicates that transmission of 36.8% or an $OD = 0.434$ will be optimal for minimizing
 5 errors due to uncertainties in transmission in two-wavelength oximetry. Expanding this further, Smith
 6 showed that the transmission range between 10% and 70% is broadly optimal for oximetry; outside this
 7 transmission range, the error function associated with measurement errors grows rapidly, so accurate
 8 oximetry becomes untenable.[44]

9 In the same study, Smith (1999) theoretically investigated the noise-sensitivity of various waveband
 10 combinations for two-wavelength oximetry, concluding that optimal waveband combinations for retinal
 11 oximetry would be 635 nm & 965 nm as well as 488 nm & 635 nm.[44] However, these theoretical
 12 waveband combinations may not be practical because they do not take into account the practical
 13 constraints of available light sources, tissue irradiance limits, pigmentation, and tissue scattering
 14 properties.

15 In practice, the optimal-wavelength combination for a given application is dictated by the calibre of
 16 blood vessels being investigated, potential sources of confounding absorption by tissue, and the
 17 constraints of the illumination and imaging systems. For two-wavelength retinal oximetry, the
 18 wavelength combination of wavebands ~600 nm (OS sensitive) and ~570 nm (isobestic) has been widely
 19 adopted. Calculated transmissions at several wavelengths of blood vessels of a range of calibers
 20 containing fully and partially oxygenated blood are shown in Figure 2. Scattering is neglected and the
 21 wavelength and caliber ranges for accurate oximetry are highlighted.



23
 24 **Figure 2.** Calculated single-pass transmissions for blood vessels at various wavebands assuming
 25 single-pass transmission and the concentration of haemoglobin to be 20 mM. (A) 100% OS, (B)
 26 70% OS. No other chromophores or optical scattering was modelled.

27 2.1.3. Corrections for blood vessel diameter and tissue pigmentation in two-wavelength oximetry

Hickam et al. (1963) noted that the observed ODR of a blood vessel is dependent on the diameter of that blood vessel.[32] Exemplar experimental data verifying this effect shown in Figure 3. It is thought that this ODR diameter-dependence is due to scattering of light and other terms which are not incorporated in the normal Beer-Lambert law, and thus not included in the theory of two-wavelength oximetry.[45] The resultant ODR offset between blood vessels of different diameters is of particular importance in experiments where blood vessels change in diameter (i.e. if the vessels dilate or contract). Stimuli such as hypoxia, hyperoxia, and, in the retina, flicker-light stimulation can cause such responses (see Section 5.3.3), and thus potentially introduce changes in ODR that are not due to changes in OS alone.

This vessel diameter-dependent effect is also problematic for oximetry of veins, which are typically larger than arteries; this can lead to a spurious decrease in venous OS estimated by two-wavelength oximetry. To compensate for this, Hammer et al., (2008) implemented an empirically-derived size-dependent venous OS correction factor.[29] A similar calibration issue is associated with tissue pigmentation: in two-wavelength oximetry, venous OS can spuriously appear to increase with increasing retinal pigmentation. Again, Hammer et al., (2008) implemented an empirically-derived, pigmentation-dependent, venous OS-correction factor to compensate for this effect.[29]

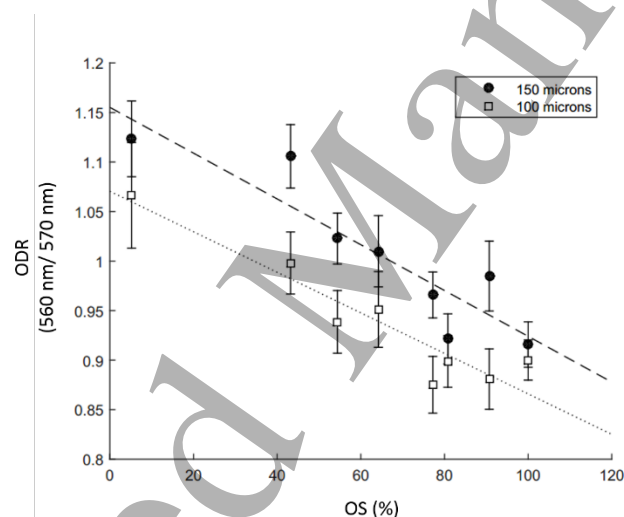


Figure 3. ODR vs. OS for fluorinated ethylene propylene (FEP) capillaries filled with *ex vivo* heparinised equine blood. The 150 μm capillary has a greater baseline ODR than the 100 μm capillary, but change in ODR for a given change in OS is approximately the same for both (fitted lines). Equipment used: FEP capillaries imaged with a retinal fundus camera modified with a snapshot multispectral imaging system. OS of *ex vivo* equine blood verified by an optical blood gas analyser [GEM OPL, Instrumentation Laboratories] with a quoted OS uncertainty of $\pm 1.8\%$ (not depicted). OS of blood was varied by addition of sodium dithionite.[46] Vertical error bars show the standard deviation of ODR along the length of the capillary section analysed.

1 2.2. Pulse oximetry

2 Pulse oximetry is widely used to non-invasively monitor arterial OS via the fingertip. Pulse oximetry
 3 uses the varying optical absorption due to pulsatile arterial blood to remove the influence of background
 4 absorbance by tissue and venous blood (assumed to be non-pulsatile); in this manner, pulse oximetry is
 5 similar to photoplethysmography.[47] Yet, by calculating the ODR of the pulsating absorbance
 6 component, two-wavelength oximetry can then be applied to estimate peripheral arterial OS.[34] To
 7 enable measurement through relatively thick tissue (i.e. in the range of one to five centimeters) pulse
 8 oximeters typically use wavelengths which are minimally absorbed and scattered by blood or tissue, e.g.
 9 650 nm and 800 nm. Pulse oximeters are calibrated across many subjects by relating average ODR to
 10 average arterial OS, as measured by an *ex vivo* blood-gas analyzer. In humans, pulse oximeters are not
 11 calibrated for OS < 80% due to ethical constraints,[48,49] and generally have an uncertainty quoted at
 12 $\pm 2\%$. [50] Pulse oximeters for animal use may, however, be calibrated for lower oxygen saturations due
 13 to less stringent ethical constraints.

14 In adult humans, the fingertip is the usual location for monitoring arterial OS, but pulse oximetry
 15 measurements can also be made via the earlobe[51] and the big toe.[52] In infants, being smaller than
 16 adults, pulse oximetry measurements can be made via alternative tissue beds, including via the palm of
 17 the hand, the sole of the foot, and the scrotum.[53,54] However, it should be noted that pulse oximeter
 18 manufacturers typically do not provide calibration for non-fingertip applications. The reliability of pulse
 19 oximeters can be reduced by low blood flow, caused by factors such as pressure on the measurement
 20 tissue, or by cold temperatures. As an example, the earlobe is particularly sensitive to reduced blood
 21 flow due to the pressure of clip-on pulse oximeters.[51] Additionally, diseases that affect the optical
 22 properties of blood, e.g. sickle cell anemia, may interfere with pulse oximetry.[55] Further, commercial
 23 pulse oximeters are often 'black box' devices with non-optional features such as time-integrated signal
 24 averaging to reduce noise in measurement. Consequently, when using pulse oximetry as a reference for
 25 MSI oximetry, the limitations of both the equipment, and the physiology of the subject should be
 26 carefully considered to ensure a relevant comparison.

27 2.3. Three-wavelength oximetry

28 2.3.1. Derivation of three-wavelength oximetry

29 Three-wavelength oximetry was developed by Pittman and Duling in 1975, and advanced the field of
 30 oximetry by incorporating optical scattering parameters into the optical transmission models of
 31 blood.[35] The technique requires three wavebands, proximal to each other in the haemoglobin
 32 absorption spectrum: two isobestic wavelengths are used to estimate the contribution by optical
 33 scattering, and a third wavelength is used for OS sensitivity.

34 The derivation of the three-wavelength oximetry model starts with the modified Beer-Lambert law:

$$35 OD_{\lambda} = \varepsilon_{\lambda} c d + B_{\lambda}, \quad 13$$

36 where B_{λ} is a term describing the effect of scattering on optical density. For two proximal wavelengths,
 λ_1 and λ_2 , B_{λ} will be approximately equal for both, i.e.:

$$37 B_{\lambda_1} = B_{\lambda_2} = B, \quad 14$$

$$\Rightarrow OD_{\lambda_1} = \varepsilon_{\lambda_1} c d + B, \quad 15$$

$$\Rightarrow OD_{\lambda_2} = \varepsilon_{\lambda_2} c d + B. \quad 16$$

38 Solving Equations 15 and 16 simultaneously yields:

$$39 B = \frac{(\varepsilon_{\lambda_1}/\varepsilon_{\lambda_2}) OD_{\lambda_1} - OD_{\lambda_2}}{(\varepsilon_{\lambda_1}/\varepsilon_{\lambda_2}) - 1}. \quad 17$$

1 It should be noted here, that if the term of $(\epsilon_{\lambda_1}/\epsilon_{\lambda_2})$ tends to 1, then minor errors in the measurement
 2 of OD will result in large errors in the estimation of B . [44] However, assuming the value of B is
 3 estimated accurately, then it can be incorporated into Equation 7 to yield:

$$OS = a \left(\frac{OD_{\lambda_3+B}}{OD_{\lambda_{ref}+B}} \right) + b, \quad 18$$

4 Where OD_{λ_3} is the optical-density at a third, oxygen-sensitive, wavelength; $OD_{\lambda_{ref}}$ is the optical-density
 5 at one of the isobestic wavelengths; and a and b are empirically derived calibration coefficients.
 6 Equation 18 has the form of the equation of a straight line, so the OD ratio can be calibrated to OS in a
 7 manner similar to two-wavelength oximetry, i.e. by plotting at least two known OS reference points
 8 versus the product of the right side of Equation 18. [35]

9 2.3.2. Discussion, and the application of, three-wavelength oximetry

10 Three-wavelength oximetry is somewhat limited in that it is only applicable for waveband triads that
 11 exhibit near-identical scattering properties, somewhat similar absorption properties, whilst including
 12 two isobestic wavebands and one OS-dependent contrast waveband. For example, Pittman and Duling
 13 (1975) [35] found that blue wavelengths (420 – 450 nm) are particularly susceptible to spurious errors
 14 in the estimation of the parameter B , due to the large variations of ϵ_{λ} , and thus large variations of
 15 refractive index, across this waveband. Instead, Pittman and Duling employed the more favourable
 16 wavelength triad of 520 nm, 546 nm, and 555 nm, reporting $\pm 1\%$ OS uncertainty for *ex vivo* blood
 17 samples. [35]

18 Smith (1999) [44] suggested the following wavelength triads as theoretically optimal for three-
 19 wavelength oximetry of retinal blood vessels: (1) 488 nm, 635 nm, and 905 nm; (2) 600 nm, 635 nm,
 20 and 905 nm; (3) 635 nm, 720 nm, and 905 nm. Whilst three-wavelength oximetry may offer improved
 21 accuracy over two-wavelength oximetry by accounting for scattering, three-wavelength oximetry still
 22 requires calibration of ODR to blood of known OS, and the choice of potential imaging wavebands is
 23 rather limited. As such, three-wavelength oximetry has been largely superseded by multispectral
 24 oximetry algorithms (see Section 2.4).

25 2.4. Multispectral oximetry

26 2.4.1. Theory and derivation of multispectral oximetry algorithms

27 Multispectral and hyperspectral[‡] oximetry algorithms estimate OS by computationally fitting
 28 experimentally determined blood vessel transmission values to a theoretical optical model incorporating
 29 OS and other optical parameters, e.g. to model the effects of optical scattering or background
 30 pigmentation. Unlike two- and three-wavelength oximetry, this optical model approach enables
 31 multispectral oximetry algorithms to be applied without implicit empirical calibration; however,
 32 validation of oximetry is a key challenge for applying multispectral oximetry (see Section 2.4.2).

33 The parameters included in multispectral oximetry models vary between studies; some parameters are
 34 “hard-wired”, and some are estimated from the recovered fit to a transmission profile. Table 1 provides
 35 a summary of hard-wired and recovered parameters in published multispectral oximetry models. As a
 36 minimum, multispectral oximetry models will “hard-wire” in the OS-dependent extinction coefficients
 37 of haemoglobin, $\epsilon_{\lambda_{O_2Hb}}$ and $\epsilon_{\lambda_{Hb}}$. Further terms may be added to account for various other parameters,
 38 including concentration of haemoglobin, blood-vessel diameter, optical-path through a blood vessel (see
 39

40 [‡] There is no formal definition of multispectral or hyperspectral imaging. Both techniques follow the same
 41 principle, but multispectral imaging typically incorporates fewer than ten wavebands, often non-continuous, and
 42 hyperspectral imaging can incorporate several tens or hundreds of contiguous wavebands (see Table 1 for
 43 examples). For simplicity, we will refer primarily to multispectral imaging in this paper.

Section 3.7), optical back scatter by blood, pigmentation of surrounding tissue, and contrast reduction due to overlying tissue and scattering by the ocular media. As a general rule, the maximum number of parameters that can be estimated to a model cannot be greater than the number of independent measurements incorporated in the model,[§] thus the more parameters that are modelled, the more wavelengths are required to apply the model. A summary of multispectral oximetry models reported in the literature, and the optical parameters they include, is provided in Table 1.

van der Putten et al. (2017) reported the most sophisticated multispectral oximetry model to date.[7] Their model builds upon the thoroughly validated model developed by Smith et al., (2000), which is applied to directly imaged blood vessels.[56] The derivation of their model starts with the Beer Lambert law:

$$OD_{\lambda} = \log_{10}(T_{\lambda}) = \varepsilon_{\lambda} C_{HbT} d, \quad 19$$

where C_{HbT} is the total molar concentration of haemoglobin. From Equation 1, $C_{HbT} = C_{O_2Hb} + C_{Hb}$, so OD_{λ} can be written as:

$$OD_{\lambda} = \varepsilon_{\lambda O_2Hb} C_{O_2Hb} d + \varepsilon_{\lambda Hb} C_{Hb} d, \quad 20$$

Rearranging gives:

$$OD_{\lambda} = C_{HbT} d [(\varepsilon_{\lambda O_2Hb} - \varepsilon_{\lambda Hb}) OS + \varepsilon_{\lambda Hb}]. \quad 21$$

To this, an additive reduced scattering coefficient μ'_{λ} (measured by Faber et al., (2004)[57]) is added to account for scattering of light by red blood cells. This gives:

$$OD_{\lambda} = C_{HbT} d [(\varepsilon_{\lambda O_2Hb} - \varepsilon_{\lambda Hb}) OS + \varepsilon_{\lambda Hb}] + \mu'_{\lambda} d. \quad 22$$

The contribution of single- and double-pass light paths through a blood vessel [58] can be accounted for by adding two multiplicative factors, α and β , representing the fraction of light rays that undergo single- or double-pass transmission respectively (see Section 3.7). Additionally, OD_{λ} can be related to transmission by $T_{\lambda} = 10^{-OD_{\lambda}}$. Therefore, Equation 22 can be rewritten as:

$$T_{\lambda} = \left[\alpha 10^{-(C_{HbT} d [(\varepsilon_{\lambda O_2Hb} - \varepsilon_{\lambda Hb}) OS + \varepsilon_{\lambda Hb}] + \mu'_{\lambda} d)} + \beta 10^{-(2C_{HbT} d [(\varepsilon_{\lambda O_2Hb} - \varepsilon_{\lambda Hb}) OS + \varepsilon_{\lambda Hb}] + 2\mu'_{\lambda} d)} \right]. \quad 23$$

To advance this model, van der Putten et al., incorporated a novel contrast-reduction parameter, K , into their multispectral oximetry algorithm. This parameter models the effects of tissue overlying a directly imaged vessel. K is described as an arbitrary increase in greyscale intensity (I_c), both in the centre of the vessel (I_v) and outside the vessel (I_o):

$$K = \frac{I_v + I_c}{I_o + I_c}. \quad 24$$

Thus, transmission can be re-written as:

$$T'_{\lambda} = \left(\frac{I_v + I_c}{I_o + I_c} \right) = T_{\lambda} (1 - K) + K. \quad 25$$

and the full optical transmission model can then be written as:

$$T'_{\lambda} = \left[\alpha 10^{-(C_{HbT} d [(\varepsilon_{\lambda O_2Hb} - \varepsilon_{\lambda Hb}) OS + \varepsilon_{\lambda Hb}(\lambda)] + \mu'_{\lambda} d)} + \beta 10^{-(2C_{HbT} d [(\varepsilon_{\lambda O_2Hb} - \varepsilon_{\lambda Hb}) OS + \varepsilon_{\lambda Hb}(\lambda)] + 2\mu'_{\lambda} d)} \right] \quad 26$$

[§] In simplistic terms, one can imagine the example of a straight-line fit, which requires at least two data points, from which two parameters – gradient and intercept – can be estimated.

$$(1 - K) + K.$$

To date, this is the most sophisticated multispectral oximetry algorithm developed and, without direct calibration, has provided plausible oximetry when utilised for *in vivo* experiments. For example, the OS of the spinal cord dorsal vein in rats was estimated to be $67.8 \pm 10.4\%$ at normoxia (mean \pm SD, $n = 4$), [7] and the OS of healthy blood vessels in murine tendons was estimated to be $\sim 95\%$. [10] Despite these encouraging results, there are still numerous challenges associated with validation of multispectral oximetry algorithms. These are discussed extensively in the next section.

Table 1. Summary of notable studies utilizing multispectral oximetry algorithms.

Study	Oximetry application	Wavebands	“Hard Wired” parameter values	Estimated parameters recovered
van der Putten et al. 2017.[7]	Rat spinal cord dorsal vein	546, 560, 570, 584, 590, and 600 nm	ϵ , S.	OS, c, S, d, K, α , β .
van der Putten et al. 2017.[9,10]	Mouse muscle tendon capillary	410, 420, 430, 435, 440, and 450 nm	ϵ , S.	OS, c, S, d, K, α , β .
Hendargo et al., 2015.[59]	Mouse skin microvasculature	540, 560, 580, and 610 nm	ϵ .	OS, c.
Clancy et al. 2015.[11]	Porcine bowel	440 – 700 nm, 28 wavebands.	ϵ .	OS, c, S.
Fernandes-Ramos et al. 2014.[5]	Red blood cells (<i>ex vivo</i>)	560 – 600 nm, 8 wavebands	ϵ .	OS, c.
Mordant et al. 2014.[19]	Retina(human glaucoma patients)	556 – 650 nm 47 wavebands	ϵ , S.	OS, c, d, α , β .
Chin et al. 2012.[13]	Diabetic foot ulcers in humans	500 – 600 nm, 15 wavebands	ϵ .	OS, c.
Yudovsky et al. 2011.[21]	Diabetic foot ulcers in humans	550 – 660 nm, 15 wavebands	ϵ , ϵ_{mel} .	Δ OS, c, ϵ_{mel} , S.
Mordant et al. 2011.[60]	Human retina	500 – 650 nm 300 wavebands.	ϵ , S.	OS, c, d, α , β .
Sorg et al. 2008. [4] and 2005.[3]	Mouse tumor model	505 – 575 nm, 16 wavebands	ϵ .	OS, c, S, α , β .
Alabboud et al. 2007.[61]	Human retina	500 – 700 nm 27 + wavebands	ϵ , S.	OS, c, d, α , β .
Smith et al. 2000.[62]	Human retina	488, 635, 670, 752, 830 nm.	ϵ .	OS, c, S, d, α , β .
Drewes et al. 1999.[63]	Human retina	629, 678, 821, 899 nm.	ϵ .	OS, c, S, d.
Schweitzer et al. 1999.[64]	Human retina	510 – 586 nm, 76 wavebands	ϵ , ϵ_{mel} .	OS, c, d, α , β .

Key: ϵ = extinction coefficient of *Hb* and *O₂Hb* ϵ_{mel} = extinction coefficient of melanin pigmentation, S = scattering contribution; c = concentration of Hb, α , β = single and double pass contribution factors respectively; d = diameter of blood vessels; K = contrast reduction factor.

2.4.2. Calibration and validation of multispectral oximetry algorithms

1
2
3
4
5
6
7 1 Potential errors in estimation of OS from MSI oximetry models, e.g. due to the influence of transmission
8 2 quantification error or ill-defined/poorly-modelled systematic parameter(s), have not been thoroughly
9 3 and robustly explored in the literature. In theory, the multi-parameter fit should minimise errors in OS
10 4 due to error in transmission measurement at a single waveband, with robustness of fit increasing with
11 5 the number of wavebands. Ideally, further research is required to quantify potential measurement errors.
12 6 Like the work of Smith for two- and three-wavelength oximetry, such error minimisation research would
13 7 likely take the form of simulations.[44] Direct experimental validation of MSI oximetry models, in
14 8 absolute terms, remains a fundamental challenge in the field of oximetry.

15
16 9 In the retina, (the vascular bed most commonly studied with oximetry) estimated OS can be compared
17 10 to well-established reference values (e.g. 96% for arteries and 54% for veins).[40] However, in many
18 11 other tissues, there are often no known absolute reference values for OS for the physiological context in
19 12 which the MSI oximetry model is being applied. Further, blood vessels of interest are typically
20 13 embedded in tissue that is both physiologically, and optically, complex; this complicates measurement
21 14 and comparison. Further, in applications such as tumor development, OS is likely to be very different
22 15 from established physiological norms due to abnormal metabolic demands.[3,4,22]

23
24 16 Healthy control subjects can be used as a qualitative reference for comparison to diseased subjects, and
25 17 to help infer inaccurate or spurious OS estimation. However, other factors such as anesthesia, local
26 18 metabolic demand, inter-subject variability, and oxygen diffusion may affect blood flow rate and OS in
27 19 healthy controls. Hence, it can potentially be challenging to verify if perceived discrepancies in OS are
28 20 due to artifacts introduced by a flawed MSI oximetry algorithm, or if they are actually due to real
29 21 physiological variations.[59]

30
31 22 In living subjects, pulse oximetry can only be used to only measure systemic arterial OS. Oxygen
32 23 sensitive nanophosphors can be used to measure local partial pressure of oxygen, but such
33 24 nanophosphors require biochemical expertise and complex phosphorescence lifetime imaging
34 25 equipment; this presents a considerable barrier to entry for researchers (see Section 5.3.2 for more
35 26 details).[65] Further, validation of *in vivo* multispectral oximetry algorithms by using artificial phantoms
36 27 may not be possible due to the significant differences in optical properties between phantom construction
37 28 materials (e.g. quartz or plastic capillaries) and real tissue (see Section 5.2 for more details on phantom
38 29 design). Oxygen-sensitive interventions that induce changes in the OS of blood, do however, allow
39 30 researchers to validate oximetry by inducing artificial changes in OS distinct from physiological norms,
40 31 enabling inter-subject comparison. Such interventions are discussed in detail in Section 5.3.3.

41
42
43 32 Fundamentally, the challenge of validating multispectral oximetry algorithms is that multispectral
44 33 oximetry algorithms are often the only method capable of providing OS measurements in many
45 34 physiological contexts, so no direct calibration with a “gold standard technique” is possible. Instead, the
46 35 field has to rely on indirect qualitative validation provided by comparison to controls, and by OS –
47 36 altering interventions to provide context for multispectral oximetry results, and build a case for
48 37 convincing oximetry measurements from context.

49 38 3. Challenges for *in vivo* multispectral imaging oximetry

50 39 3.1. *Optical absorption by haemoglobin variants and blood plasma*

51
52
53
54 40 For understanding errors and uncertainties in oximetry, it is useful to consider the optical properties of
55 41 blood constituents, other than haemoglobin (Hb), which may absorb or scatter light, and how these may
56 42 alter the optical transmission of blood vessels. For example, variant globin proteins, blood plasma, and
57 43 cells within blood.

1 Haemoglobin has two main variants, namely methemoglobin (MetHb), where the iron in heme groups
2 is Fe^{3+} instead of Fe^{2+} , and carboxyhemoglobin (CoHb), where carbon monoxide is bound to
3 haemoglobin. If present in the blood, MetHb and CoHb can contribute spectral absorption that is similar
4 to normal Hb.[66–68] However, the concentration MetHb and CoHb are normally present only at low
5 concentration in blood and are thus generally ignored for oximetry.[68] Another molecule similar to Hb
6 is neuroglobin, which supplies oxygen to nervous tissue, such as the brain and retina.[69] However, the
7 extent to which neuroglobin can be found in the blood is currently unclear.[70–72] Other proteins similar
8 to Hb can sometimes be found in the blood. For example, myoglobin (Mb) – a protein which supplies
9 oxygen to muscle tissue – can be found in blood when a subject has undergone skeletal or cardiac muscle
10 damage, e.g. due to a heart attack or traumatic injury.[73,74] The absorption spectra of Mb is broadly
11 similar to Hb, but with weaker optical absorption because Mb contains only a single heme group
12 compared to the four heme groups of Hb.[75] Mb is not considered in MSI oximetry, even in
13 experiments that may cause muscle damage.

14 White blood cells account for <1% of whole-blood volume, but do not contribute significant absorption
15 or scattering,[76] and are not considered in oximetry. However, blood plasma is ~55% of the total
16 volume of human blood, and contains many proteins which can absorb and scatter light.[77] When
17 isolated from whole-blood, blood plasma has a pale-yellow coloration due to strong absorption by serum
18 albumin at wavelengths < 550 nm. Additionally, blood plasma auto-fluoresces under ultraviolet and blue
19 light exposure, [78] which could potentially induce errors in oximetry (see Section 3.4 for more on auto-
20 fluorescence). However, to the best of our knowledge, no oximetry studies to date have incorporated the
21 optical parameters of blood plasma.

22 3.2. Pigmentation within tissue

23 Melanin is the main pigment chromophore** of concern for oximetry. Melanin strongly absorbs blue
24 and green light, with red light less strongly absorbed.[79] If present in high concentration, absorption
25 by melanin may be sufficient to make meaningful MSI oximetry challenging. Melanin is particularly
26 abundant in the skin and retina, and as such, is particularly relevant for oximetry of blood vessels in
27 these tissue beds. Retinal melanin can be quantified via the proxy of assessment of iris coloration;
28 subjects with low retinal melanin tend to have blue iris coloration, whereas subjects with a high degree
29 of retinal melanin tend to display brown iris coloration.[80]

30 The non-uniform distribution of melanin in retinal tissues introduces considerable variability in the
31 reflectivity of background for blood vessels, compromising oximetry measurements. For this reason,
32 Hammer et al., (2008) introduced an empirically derived calibration factor to account for the effect of
33 retinal melanin pigmentation in two-wavelength oximetry.[29] In subjects with minimal retinal melanin
34 pigmentation, the retinal tissue is so transparent that the blood vessels of the choroid – at the back of the
35 retina – can be directly studied by MSI oximetry.[14]

36 Other chromophores such as adipose fat and yellow pigment could affect the spectra of tissue at visible
37 wavebands, but the influence of such pigments is not normally accounted for in oximetry. Absorption
38 by water is not typically a concern for oximetry, because water only strongly absorbs light at >1000 nm,
39 which is beyond the waverange of 400 – 800 nm typically used for oximetry. A thorough review on
40 absorption and scattering properties of these miscellaneous tissue chromophores is provided by Jacques
41 et al., (2013).[79]

42
43
44
45
46
47
48
49
50
51
52
53
54
55
56
57
58
59
60
** A chromophore is a molecule that absorbs visible light, responsible for the characteristic colour of a substance when viewed with the eye.

1 3.3. Optical scattering by tissue

2 Optical scattering by tissue is due to inhomogeneities in the refractive index of the tissue, e.g. cells or
3 blood vessel walls. Consequently, such scattering is well-described by Mie scattering theory, where the
4 scattering structures are similar in dimension to the wavelength of light being scattered. Unlike Rayleigh
5 scattering, Mie scattering does not strongly vary with wavelength, but becomes more important when
6 absorption is reduced, e.g. at red and near-infra red wavelengths. The scattering properties of the
7 skin,[81–83] the retina,[84,85] the sclera,[86] and blood[87] are well characterised.

8
9 Optical scattering by overlying tissue can alter the transmission of blood vessels.[7] For example, in the
10 tissue of the choroid, scattering results in blood vessel appearing to be brighter than the surrounding
11 tissue, producing a negative OD. This is particularly apparent when the reflectivity of surrounding tissue
12 is low. In such situations, two-wavelength oximetry calibration is not applicable, but nevertheless
13 indications of relative OS may instead be reported in terms of ODR.[14] The best example of this
14 phenomenon has been reported by Kristjansdottir et al., (2013).[14]

15 Although generally unavoidable, scattering by skin tissue can be reduced by the application of optical
16 clearing substances, which match the refractive index of inhomogeneities within tissue, thus reducing
17 scattering. Optical clearing agents are typically used to reduce scattering in skin to provide deeper and
18 clearer optical imaging, however, they may alter various tissue properties, and may require invasive
19 injections for maximum effectiveness.[88,89] Hence, optical clearing agents are not commonly used in
20 oximetry experiments.

22 3.4. Other challenges of imaging through tissue

23 Aside from absorption by chromophores and optical scattering, there are other challenges associated
24 with imaging blood vessels through tissue, including limited depth penetration of light, tissue-specific
25 wavelength filtering effects, polarization dependent effects, tissue geometry, and tissue auto-
26 fluorescence.

27
28 The penetration depth of light in tissue is highly variable, with blue and green wavelengths generally
29 limited to a penetration depth of < 2 mm due to strong absorption and scattering.[90,91] However,
30 wavelengths between 600-1000 nm can pass further through tissue due to reduced absorption at these
31 wavelengths, enabling applications such as pulse oximetry. This waveband is sometimes referred to as
32 “the biological window”. Photoacoustic imaging techniques get around this limit by combining optical
33 excitation with ultrasonic detection (see Section 6.4).

34
35 Specific tissue may also have associated wavelength-filtering effects: for example, the lens within the
36 human eye acts as an ultraviolet filter, with the transparency of the lens decreasing across all wavelengths
37 with age.[92] Cataracts can also influence oximetry measurement by effectively applying a spectral-
38 filter function over images, consequently altering ODR of blood vessels imaged within the eye.[93,94]

39
40 Tissues may also exhibit birefringence, caused by parallel strands of fibrous tissue. In the eye, the sclera,
41 the cornea, and the retinal nerve fibre layer are generally birefringent.[95–98] Birefringence is
42 particularly important for studies utilising orthogonally polarised illumination to mitigate reflections
43 (see Section 3.7) because birefringence can result in uneven tissue reflectivity that can cause challenges
44 for oximetry.

45
46 Defocus due to tissue curvature or bulk motion can significantly reduce the apparent contrast of blood
47 vessels with respect to other features. Defocus due to tissue curvature is a particular challenge for both

1 endoscopic and ocular imaging. To minimise defocus, retinal oximetry studies typically limit
 2 measurements to a well-defined, well-constrained region near the optic disc[99]; when imaging the
 3 surface of the eye (the sclera), maximising the depth of field is a good strategy for minimising any
 4 potential defocus.[100]

5
 6 Some tissues may exhibit auto-fluorescence when illuminated with the appropriately exciting
 7 wavelengths (typically ultraviolet or blue light). For example, proteins within blood plasma will strongly
 8 auto-fluoresce under blue illumination (e.g. ~400 nm), and emit at longer wavelengths (e.g. ~500
 9 nm),[78] and auto-fluorescence of retinal tissue (excitation ~ 470 nm, emission at ~600 nm) is strong
 10 enough to be utilized as a retinal imaging modality in its own right.[101] To date, auto-fluorescence has
 11 not yet been considered as a source of potential errors in oximetry, but nevertheless it is prudent to be
 12 wary of, and minimise, any tissue auto-fluorescence in oximetry experiments.

13 3.5. Scattering by blood

14 3.5.1. General considerations

15 Optical scattering by blood should be considered when interpreting transmission of blood vessels for
 16 oximetry. In blood, light is predominately Mie scattered by individual red blood cells (RBCs) which
 17 make up approximately 44% of total-blood-volume, and which are each ~6 – 8 μm in diameter with a
 18 concave shape (see Figure 4).[77] Proteins in blood plasma also contribute Rayleigh scattering effects,
 19 but the magnitude of this scattering is 100-1000 times less than scattering from RBCs.[77] The scattering
 20 properties of blood can alter due to several factors, including: changes in OS,[102] change in % of RBCs
 21 by volume (the haematocrit),[103] changes in overall blood volume (e.g. due to water drinking),[104]
 22 and changes in blood flow rate.[64,105]

23
 24 The quantitative parameters that describe the scattering of light by blood are the absorption coefficient
 25 (μ_a) [units: $\text{cm}^{-1}\text{M}^{-1}$]; the scattering coefficient (μ_s) [units: cm^{-1}]; the anisotropy factor (g)
 26 [dimensionless]; and the effective scattering coefficient: $\mu'_s = \mu_s(1 - g)$ [units: cm^{-1}].[77] The
 27 anisotropy factor is defined as: $g = \cos(\theta)$, where θ is the typical angle at which incident light is
 28 deflected by a scattering event. $g = 0$ indicates no forward scattering, and $g = 1$ indicates complete
 29 forward-scattering. For whole blood, g has been estimated to be ~ 0.985 - 0.997, i.e. highly forward-
 30 scattering.[57]



31
 32
 33
 34
 35
 36
 37
 38
 39
 40
 41
 42
 43
 44
 45
 46
 47
 48
 49
 50
 51
 52
 53
 54
 55
 56
 57
 58
 59
 60
Figure 4. Depiction of red blood cells showing their biconcave shape. *Figure reproduced from the public domain.*[106]

32 3.5.2. The influence of oxygen saturation on optical scattering by blood

OS plays a role in determining the optical scattering properties of blood by mediating the transmission of blood. Monte Carlo simulations by Friebe et al., (2009) demonstrated that an increase in ϵ_{λ} will decrease g . Thus, if a change in OS results in a decrease in the optical transmission of blood, then the degree of forward scattering through blood will also decrease, resulting in a further decrease in transmission, not described by the Beer-Lambert law.[102]

3.5.3. The influence of blood flow speed on scattering and reflection by blood

The orientation of RBCs within flowing blood is dependent on blood flow velocity: if blood is static or flowing very slowly, then RBCs will be randomly orientated, and biconcave in shape. However, if blood is flowing, then RBCs will preferentially align with the flow, and elongate in the direction of flow due to shear stress (see Figure 5).[107] This alignment consequently alters the optical properties of blood, particularly backscattering. Klose et al., (1972) demonstrated that preferential alignment of RBCs under flow results in an increase of backscattered light from blood vessels.[105] Schweitzer et al., (1999) demonstrated that once all RBCs are orientated in the same direction, then the back-scattered light would reach a maximum. For a 50 μm diameter blood vessel, this critical flow speed corresponding to complete preferential alignment was found, empirically, to be 6.4 mm/s.[64] Thus, it is important that blood flow speed is considered in oximetry experiments because blood at low, moderate, and critical flow rates will have different optical back-scattering properties. Back-scattering from blood can produce specular reflections, which can introduce errors into oximetry (see Section 3.6).

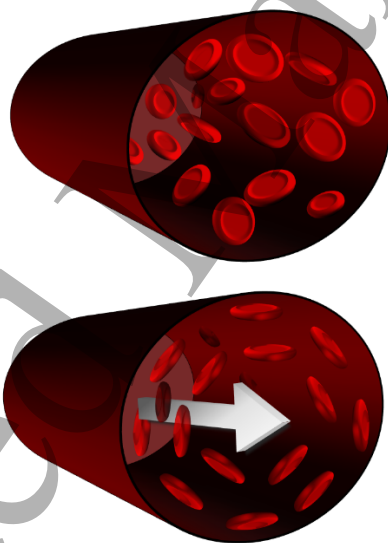


Figure 5. Depiction of the preferential alignment of red blood cells under flow due to shear stress. Top: no flow. Bottom: under flow. A more detailed depictions of this phenomenon can be found in Cimalla et al., (2011).[107] Note, this depiction describes a relatively large blood vessel (e.g. 100-200 μm diameter), and is not valid in capillaries (<10 μm in diameter) where red blood cells elastically deform to flow through capillaries.[108]

3.6. Mitigating specular reflections from blood vessels

Illumination light can create a bright specular reflection from the surface of a blood vessel, typically manifesting in the centre of a vessel (see Figure 6). Such specular reflections can introduce errors in the estimation of transmission of a blood vessel and thus induce errors in MSI oximetry (see Figure 6). There are several methods for mitigating specular reflections. One strategy is to use off-axis illumination

of blood vessels, thus moving the position of specular reflections to a less intrusive angle. However, off-axis illumination creates shadowing effects and is impractical for many *in vivo* applications, such as retinal imaging, where off-axis imaging requires invasive procedures.[109] Another, simpler, approach is to modify blood vessel transmission-measurement algorithms to compensate for reflections. With this approach, the potential for systematic errors should be carefully considered. Alternatively, annular illumination can be employed to back-illuminate blood vessels via diffuse scattering via surrounding tissue; totally eliminating specular reflection from the blood vessel.[110]

Perhaps the most elegant approach to mitigate specular reflections is to use orthogonal polarization imaging (OPI). In OPI the illumination light is linearly polarised, but becomes depolarized when it undergoes multiple scattering by tissue. In contrast, specularly reflected light, does not lose its polarization because it does not undergo multiple scattering. Thus, by placing a linear polariser in the imaging path, with its polarization axis orientated orthogonally to the polarization axis of the illumination light, specular reflections can be completely mitigated, whilst light that has undergone multiple scattering by tissue is imaged.[111]

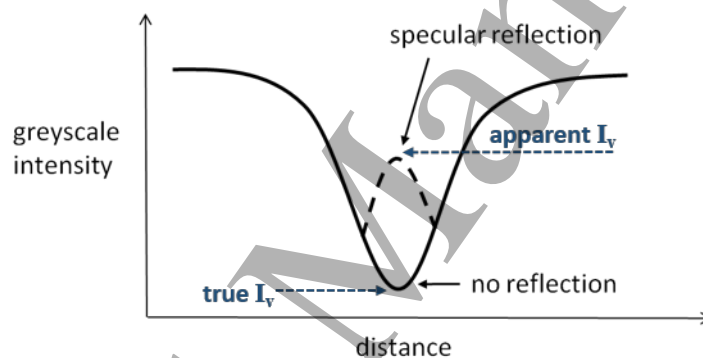


Figure 6. An ideal blood vessel intensity-profile cross section, with and without specular reflection. Specular reflections increase the apparent intensity (I_v) in the centre of a blood vessel.

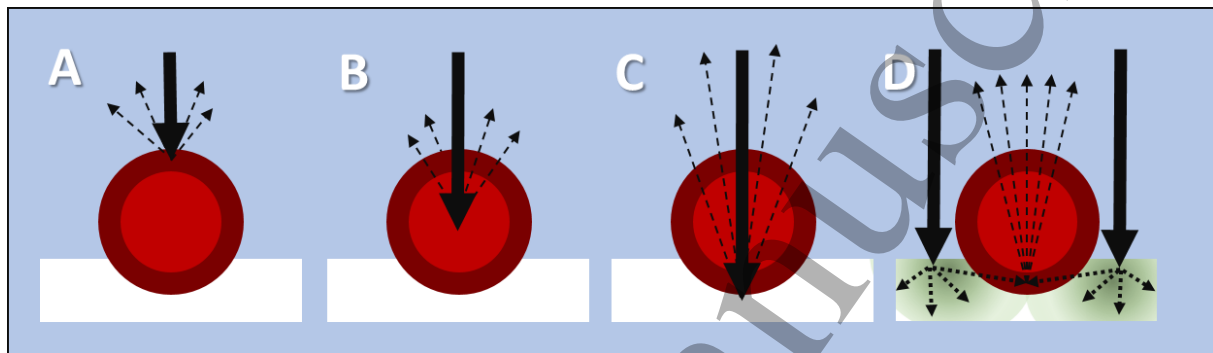
3.7. Optical paths through blood vessels

Light does not simply follow a single path through blood vessels; scattering, reflection, absorption all play a role in determining the path of individual photons through blood. Scattering is described in terms of scattering probabilities, with the outcome of each event determined in a pseudo-random manner. Hence, Monte Carlo simulations are a useful method for investigating light paths through blood vessels because they simulate many individual photons propagating through blood. Predictions by Monte Carlo models can be compared to experimental data to assess optical models or to test predictions of parameters, e.g. the scattering anisotropy factor of blood, g (see Section 3.5.1).

Hammer et al., (2001) [112] used Monte Carlo simulations to investigate different light paths through blood vessels when the blood vessels were illuminated by retinal fundus cameras and scanning laser ophthalmoscopes (SLOs). Simulations were conducted for light in the waveband 520 -586 nm and investigated model blood vessels 25 – 200 μm in diameter. Examples of the light paths through blood vessels simulated in this study are shown in Figure 7. They found that back-scattered and single-pass transmitted light dominates for both fundus cameras and SLOs. However, compared to fundus cameras,

1 SLOs have a higher degree of backscattered light, with a relatively larger double pass transmission
2 contribution.[112]

3 Rodmell et al., (2014)[110] conducted Monte Carlo simulations to investigate if vessels can be diffusely
4 illuminated by illuminating nearby tissue, instead of directly illuminating blood vessels, e.g. by using a
5 confocal SLO illumination scheme. Their study concluded that if the tissue surrounding a vessel is
6 illuminated, then the vessel will be effectively back-illuminated.[110] This finding has subsequently
7 been used to simplify multispectral oximetry models by enabling the use of annular illumination to
8 eliminate double-pass contributions in MSI oximetry models.[9,70]

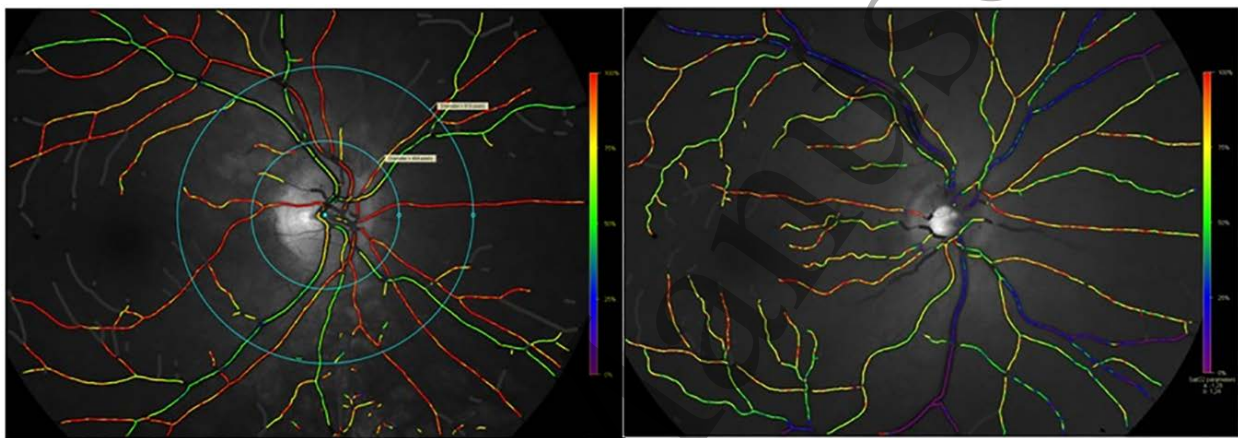


10

1 **Figure 7.** Potential light paths through a blood vessel. (A) specular reflection. (B) backscattered. (C)
 2 double pass. (D) Single-pass (back illuminated).[112]

3 3.8. Rattlesnake artefacts

4 A common artefact in oximetry is “rattlesnaking”, where estimated OS spuriously varies along the
 5 length of a blood vessel, causing a stripey, “rattlesnake” pattern to appear when OS is visualized as a
 6 colour-coded map (see Figure 8). Spurious variations in estimated blood vessel transmission can arise
 7 due to a number of reasons, including variations in red blood cell concentration, optical scattering,
 8 background pigmentation, and vessel-fitting errors. To minimize the adverse effects of rattlesnaking,
 9 OS is often averaged along the length of a blood vessel or vessel segment to reduce random variations
 10 in OS prior to further analysis.



11 **Figure 8.** Two-wavelength retinal oximetry images of a healthy subject (left) and a subject with chronic
 12 obstructive pulmonary disorder (right). Rattlesnaking artefacts are apparent in both subjects. Figure
 13 reproduced from Eliasdottir et al., (2017) under a Creative Commons BY 4.0 licence.[113]

15 3.9. Oxygen diffusion

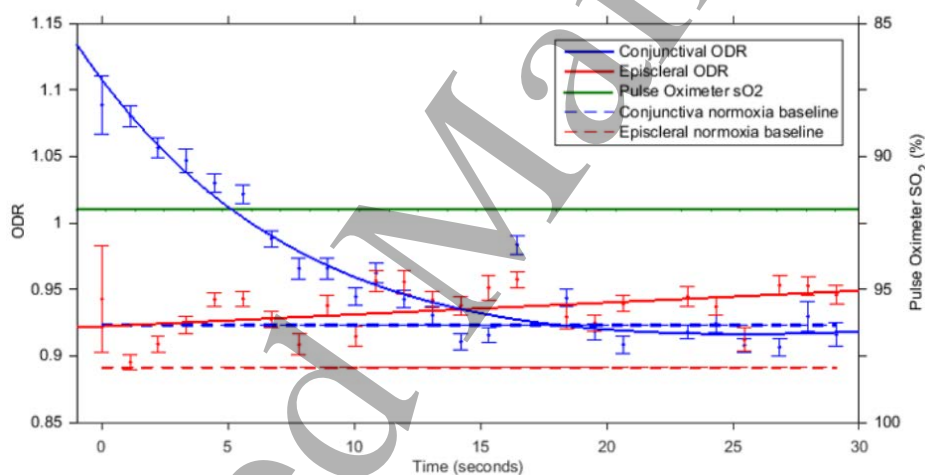
17 Oxygen diffusion has recently emerged as both a challenge and a tool for oximetry of blood vessels
 18 exposed to ambient air, e.g. in bulbar conjunctival and tendon oximetry.[10,15] Oxygen will naturally
 19 move from regions of high partial pressure of oxygen (pO_2) (e.g. the air) to areas of lower pO_2 (e.g.
 20 exposed blood vessels), until a pO_2 equilibrium is reached. This will raise the OS of blood. Nominal pO_2
 21 of blood is ~ 100 mmHg and ~ 40 mmHg for arteries and veins respectively, whereas nominal pO_2 of
 22 air at sea level is much higher, at ~ 160 mmHg.[27] Therefore, if blood reaches equilibrium with ambient
 23 air, then the OS of blood will be close to 100%. The rate of oxygen diffusion for air to blood is described
 24 by Fick's law of diffusion, which incorporates two main factors: the pO_2 gradient, and the oxygen
 25 diffusivity of any tissue between the air and the blood. The oxygen diffusivity of tissues depends on
 26 tissue thickness and composition.[114–117]

27 Oxygen diffusion will occur when blood vessels are exposed to the ambient air. For example, in the first
 28 MSI oximetry study of the bulbar conjunctival microvasculature (located on the surface of the eye),
 29 MacKenzie et al., (2016)[15] observed rapid oxygen diffusion from ambient air into hypoxic bulbar
 30 conjunctival microvessels when the eyelid was open. This oxygen diffusion occurred in a timescale of
 31 just a few seconds, with 50% of the oxygen diffusion occurring on average in 3.4 ± 1.4 seconds (see
 32 Figure 10). Closure of the eyelid created a barrier to oxygen diffusion from ambient air. Due to this
 33 oxygen diffusion, it is thought that all bulbar conjunctival vessels will be highly oxygenated when
 34 exposed to air after a few seconds.[15]

1 This diffusion oxygenation effect has been exploited by other studies. Sarkar et al., (2017) exploited
 2 oxygen diffusion to remove OS as a source of uncertainty in their experiments to non-invasively measure
 3 bulbar conjunctival haemoglobin concentration for anemia diagnosis.[118] van der Putten et al.,
 4 (2017)[9] utilized reoxygenation by diffusion as an intervention to alter OS and confirm oximetry
 5 capability.[9] It has been suggested that oxygen diffusion rates could be investigated as a parameter for
 6 the measurement of microvascular function, e.g. to investigate vessel wall thickening due to diabetes,
 7 but further research on this matter is required.[15]

8 Oxygen diffusion is a concern in studies where blood vessels are surgically exposed, because oxygen
 9 diffusion can spuriously increase blood OS. A test for ongoing oxygen diffusion into surgically exposed
 10 venules was reported by van der Putten et al., (2017)[7] They reasoned that if oxygen diffusion was
 11 occurring, then blood would become more oxygenated as it flowed down the length of a vein. In their
 12 particular case, van der Putten et al. did not observe an OS gradient along the length of veins examined.
 13 indicating no significant oxygen diffusion into these veins.[7]

14 In the retina, oxygen diffusion is not a concern, because retinal blood vessels are shielded from air by
 15 the tissue of the eye. However, the potential effects of oxygen diffusion should be carefully considered
 16 in any oximetry application where blood vessels may be exposed to air. For example, if invasive
 17 intravitreal retinal illumination is used, then diffusion may cause spurious changes in OS.[109]



18 **Figure 9.** Oxygen diffusion from ambient air causes rapid reoxygenation of hypoxic
 19 bulbar conjunctival blood vessels (blue line). The ODR of episcleral vessels (red line)
 20 and fingertip pulse oximeter OS (green line) remain constant because these blood vessel
 21 beds are embedded within tissue and thus do not undergo diffusion. The x-axis is
 22 elapsed time after the subject opens their eyelid. Error bars represent the standard error
 23 of the mean. For clarity, pulse oximetry error bars of $\pm 2\%$ OS are not shown. NB: in
 24 this diagram SO_2 denotes OS. Figure reproduced from MacKenzie et al., 2016 with
 25 permission.[15]

27 3.10. Multi-OS laminar flow in trunk veins

28 It is common for multiple tributary venules to merge into a single larger, trunk vein. This results in
 29 multiple non-mixing, laminar, blood streams of varying OS flowing within trunk veins, producing a
 30 heterogeneous OS distribution. This will introduce errors into the estimation of OS, because all oximetry
 31 algorithms to-date assume a single homogenous OS across the breadth of a vessel.
 32
 33

This multi-OS laminar flow phenomenon is most readily observed during retinal fluorescein angiography, but can also be verified with flow-sensitive optical coherence tomography,[119] and multispectral imaging.[59] Hendargo et al., (2015) have provided the clearest demonstration of the multi-OS laminar flow problem.[59] However, at the time of writing, no method to estimate and/or compensate for the error due to this multi-OS laminar flow has been developed.

4. Image processing for multispectral imaging oximetry

4.1. Image acquisition

Image acquisition for multispectral imaging generally follows best practice for general scientific imaging in that images should be well-exposed so as to have a good signal to noise ratio, dark current and random noise in the detector should be accounted for, and images should be acquired at the highest possible bit-depth to ensure maximum sensitivity to changes in intensity across the scene. Additionally, images should be saved in uncompressed format (e.g. *.TIFF*), because saving images in a compressed format (e.g. *.jpg*) can result in artefacts (see Figure 10).

Sensitive monochromatic scientific detectors (e.g. CCDs and CMOS detectors) are best suited for MSI oximetry due to their low noise levels, high sensitivity, fast read out rates, and generally good hardware to control software connectivity. Some oximetry studies have utilized consumer single lens reflex (SLR) cameras as detectors, although good software control and high data acquisition rates are typically harder to achieve compared to scientific detectors.[7]

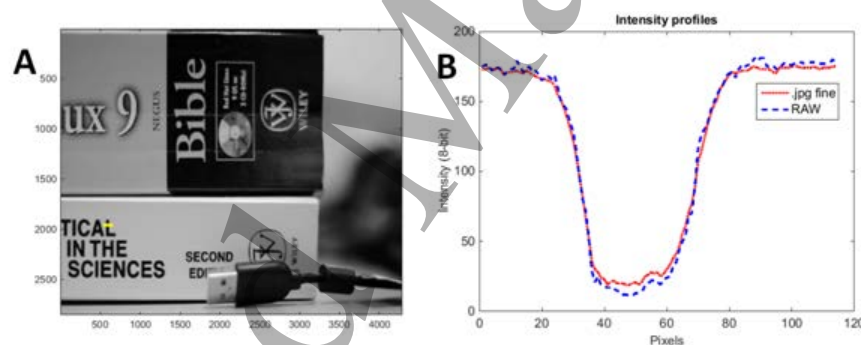


Figure 10. The scene in sub-figure A was acquired simultaneously in two image formats: *RAW* (uncompressed) and *.jpg fine* (compressed). The yellow line indicates the line-profile selected for analysis. **(B)** The corresponding intensity line-profile can be seen to differ between formats, with the *.jpg* image showing increased apparent intensity at the centre of the line profile. If this line profile were of a blood vessel, these *.jpg* compression artefacts would result in a different estimation of blood vessel transmission, and thus introduce systemic errors in the estimation of OS.

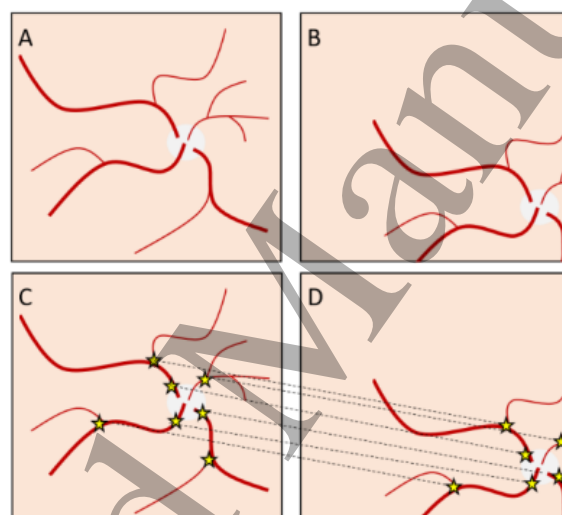
4.2. Co-registration of multispectral images

Prior to MSI oximetry analysis, co-registration of multispectral images is essential to ensure that the same region of a blood vessel is analyzed in each image at a different waveband. Broadly speaking, there are two main classes of multispectral image co-registration algorithms: feature-matching co-registration and cross-correlation co-registration.

1 4.2.1. Feature-matching co-registration algorithms

2 Feature-matching algorithms are best applied to co-registration of “feature-rich” images: i.e. images
 3 with features that exhibit strong contrast and distinct boundaries. In brief, feature-matching algorithms
 4 detect distinct features in different images, determine which points corresponds to detected points in
 5 other images, estimate the relative displacement of these matching points, and then compute a
 6 corresponding affine transform to apply operations such as rotation, scaling, shear, and reflection;
 7 resulting in co-registration of the two images (see Figure 11). Affine transforms are defined as
 8 transforms that preserve linearity of features, along with the ratio of distances.[120]

9 For feature-matching co-registration algorithms to perform well, a large number of potential registration
 10 points must be used, requiring numerous distinct features. However, automatically identifying enough
 11 distinct features can be highly challenging in biological imaging. For example, feature-matching
 12 algorithms can struggle to detect blood vessels across different wavebands, because the contrast of blood
 13 vessels compared to background tissue varies greatly between green and red wavebands (see Figure 12).



14
 15
 16
 17
 18
 19
 20
 21
 22
 23
 24
 25
 26
 27
 28
 29
 30
 31
 32
 33
 34
 35
 36
 37
 38
 39
 40
 41
 42
 43
 44
 45
 46
 47
 48
 49
 50
 51
 52
 53
 54
 55
 56
 57
 58
 59
 60

Figure 11. Principle of a feature-matching image co-registration algorithm. (A) Main image. (B) Arbitrarily displaced image. (C) Distinct unique features identified are identified. (D) Matching distinct and unique features are identified in image B, and used to compute an image transform to co-register images A and B.

15

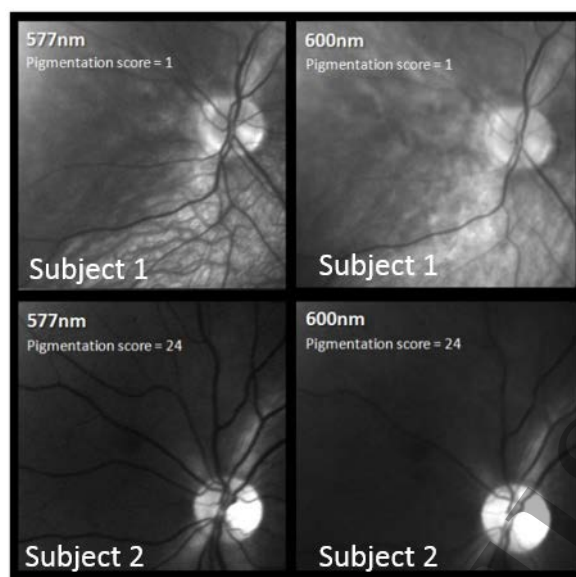


Figure 12. Retinal images of two different subjects at 577 nm and 600 nm. **Top:** a subject with a low degree of retinal pigmentation. **Bottom:** a subject with a high degree of retinal pigmentation. The bright white region is the optic disk.

1 4.2.2. Cross-correlation co-registration algorithms

2 Unlike feature-matching algorithms, cross-correlation image co-registration algorithms can be applied
3 to images with poor feature contrast. However, this comes with the requirement of considerably more
4 computational processing time than feature-matching algorithms. Cross-correlation-based registration
5 algorithms work by overlaying two images and calculating the cross-correlation function of the two
6 images, which can be calculated rapidly by fast Fourier transform techniques. The algorithm will then
7 iteratively apply incremental transforms in one of the images, checking the cross-correlation function
8 after each iteration, until a global maximum is reached. However, reaching a global maximum can
9 require many iterations of image transformation, and thus can be computationally time-
10 intensive.[61,121] A logic flow-chart for a cross-correlation algorithm is shown in Figure 13.
11

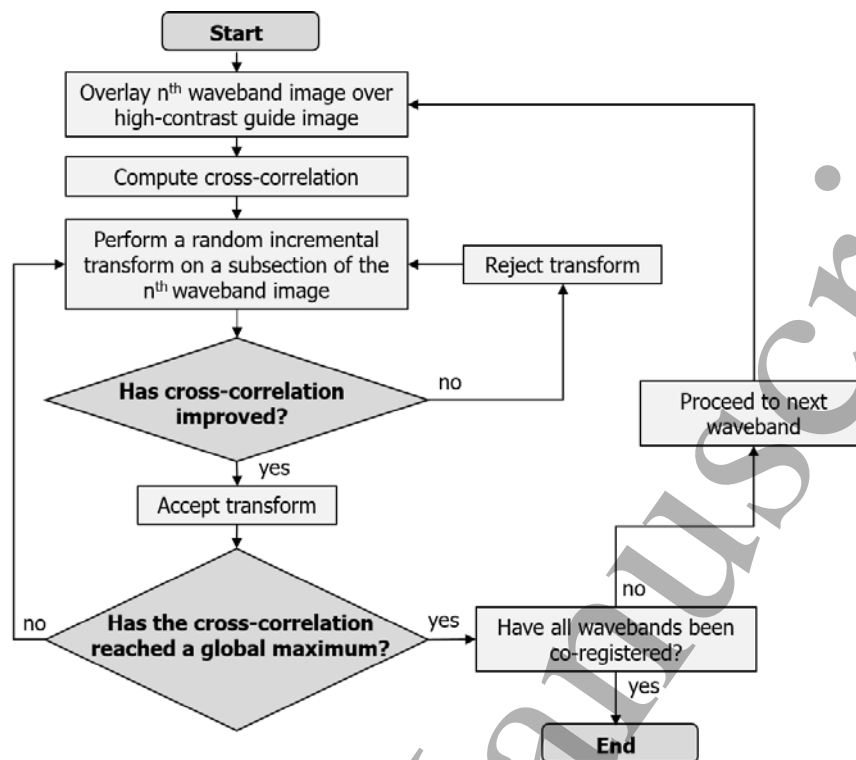


Figure 13. An exemplar logic flow-chart for a cross-correlation image co-registration algorithm. Rectangular nodes represent operations. Diamond nodes represent decision points.

1

2 4.2.3. Other challenges of *in vivo* image registration

3 Automatic image registration algorithms rely on the assumption that features in the scene are
 4 unchanging. This assumption is not always true, especially when using time-sequential MSI *in vivo*. For
 5 example, subject motion can introduce motion blur or defocus,[122] and conjunctival blood vessels are
 6 semi-mobile relative to background tissue.[15] In such challenging circumstances, semi-automatic
 7 registration using human input may be required to successfully identify features for successful co-
 8 registration.[123]

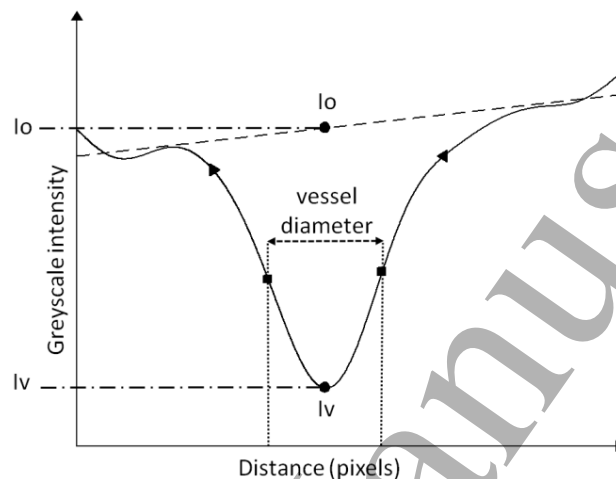
9 4.3. Estimating the transmission of blood vessels

10 Estimation of the transmission of a blood vessel requires the measurement of three parameters:

- 11 1. The intensity of light at the centre of the blood vessel (I_v)
- 12 2. The intensity of light in the position corresponding to the centre of the blood vessel, if the
 13 blood vessel were not present (I_o).
- 14 3. The diameter of the blood vessel.

15 The typical approach to estimate these parameters is to analyse an intensity line profile across the blood
 16 vessel and nearby tissue, orthogonal to the direction of blood flow. The length of the line profile is
 17 arbitrary, but as a rule of thumb, a line profile length equivalent to three times the blood vessel diameter
 18 should suffice. Fischer et al., (2010) [124] proposed an algorithm to estimate the blood vessel diameter
 19 by defining the blood vessel walls as being the points in a line profile corresponding to greatest rate of

1 change of intensity.[124] . I_v is typically estimated by fitting a function such as a Gaussian or parabola
 2 to the inside of a blood vessel, and recovering the intensity at the centre of the vessel. I_o is typically
 3 estimated by plotting a linear fit to the surrounding tissue and extrapolating this linear fit to find the
 4 intensity at the position corresponding to the centre of the vessel. Figure 15 shows an example of a line
 5 profile fitting scheme. Further examples of line profile fitting with real line profiles can be found in van
 6 der Putten et al (2017).[5]
 7



8 **Figure 14.** Depiction of a vessel profile fitting
 9 scheme to estimate vessel diameter, and intensity
 10 inside the vessel (I_v) and the background intensity
 11 if the vessel were not present (I_o). Reproduced with
 12 permission from MacKenzie et al., (2016).[15]
 13

8 5. Strategies for validation of multispectral imaging oximetry

9 For many applications, MSI oximetry is the only oximetry technique capable of measuring OS in the
 10 blood vessels under investigation; no “gold standard” reference technique is available. Instead, MSI
 11 oximetry has to rely on somewhat indirect methods of validation. This section describes the various
 12 techniques which have been employed to validate oximetry and related assumptions.
 13

1 5.1. Testing fundamental optical assumptions: Monte Carlo Simulations

2 MSI oximetry algorithms incorporate multiple optical parameters to estimate changes in blood vessel
3 transmission due to OS (see Section 2.4). Some parameters, such as the extinction coefficient of
4 chromophores, can be “hard-coded” from empirically measured values. However, other parameters,
5 such as the degree of single pass and double pass light path contributions are challenging to estimate
6 from experiments. Computational Monte Carlo simulations have been utilized as a method for testing
7 and validation of optical assumptions which would otherwise be highly challenging or not possible to
8 experimentally verify. However, Monte Carlo simulations have some drawbacks, mainly the expertise
9 and expense associated with using computational simulation software. Additionally, researchers must
10 be sure that the simulation software incorporates all relevant biological and optical parameters (e.g.
11 tissue scattering functions) that are required for comprehensive optical simulation. For examples of how
12 Monte Carlo simulations have been used to test assumptions in oximetry, refer to Sections 3.5.2 and 3.7.

13 5.2. Validation with artificial phantoms

14 Phantoms are artificial constructs designed to mimic blood vessels and tissue, for the purpose of testing
15 oximetry measurements in “well controlled”^{††} scenarios. Phantoms typically incorporate *ex vivo* blood,
16 with OS of that blood controlled by one of three methods: (1) bubbling oxygen-free gas through blood
17 (e.g. Nitrogen or Argon) [125,126]; (2) by addition of a chemical such as sodium dithionite [46] or
18 sodium bicarbonate [127]; or (3) by introducing an oxygen consuming micro-organism, such as yeast,
19 to the blood.[128] OS of *ex vivo* blood can be verified by an *ex vivo* blood gas analyzer or partial pressure
20 of oxygen probe, giving a useful comparison point for MSI oximetry.

21 The design and construction of phantoms for MSI oximetry varies considerably depending on the tissue
22 being simulated and MSI modality. For example, a retinal oximetry phantom may consist of blood-filled
23 capillaries within a water-filled model eye.[129] whereas a photoacoustic imaging phantom may consist
24 of a thick gelatinous agar slab with blood-filled capillaries embedded within. Phantoms can also contain
25 embedded test-targets to verify imaging performance.[130] Complex flow-cells designed to mimic the
26 microcirculation in both flow speed and oxygen extraction have also been fabricated.[126] A full review
27 of MSI phantoms across all modalities is beyond the scope of this tutorial, but a summary of phantoms
28 for MSI oximetry in the eye can be found in Mackenzie et al., (2017).[6]

29 5.3. In vivo validation strategies

30 5.3.1. Blood gas measurement and pulse oximetry

31 Blood gas analysis of *ex vivo* blood samples from large blood vessels (e.g. the antecubital vein) was the
32 first technique used to validate *in vivo* retinal oximetry.[32] However, direct blood sampling is now
33 rarely done due to several reasons: 1. Invasive procedures that cause a risk of harm to a subject should
34 be avoided wherever possible [131];^{‡‡} 2. Suitably qualified staff are required to draw blood from a
35 human subject; 3. Pulse oximetry has provided a quick, convenient, and non-invasive alternative in
36 humans (as well as other animals); and 4. a standardized set of reference OS values has been adopted
37 for two-wavelength retinal oximetry.[40] However, *ex vivo* blood gas measurement may be used in
38 animal studies, where animal handling is done exclusively by suitably-trained and suitably-licensed
39 individuals.[132]

^{††} Blood behaves quite differently *in vivo* and *ex vivo*; effects such as RBC aggregation are apparent in *ex vivo* blood but not *in vivo* blood. As such, phantoms utilising *ex vivo* blood are not necessarily “well controlled” in the traditional sense, but such phantoms do offer researchers control over key variables, e.g. OS, to a degree not possible in *in vivo* experiments.

^{‡‡} Medical research involving human subjects must be carried out in accordance with the tenants of The Declaration of Helsinki, as set out by the World Medical Association.[131]

1
2
3
4
5
6
7 1 In humans, pulse oximetry can be applied to the fingertip and earlobe, whereas paw and carotid artery
8 2 pulse oximeters are available for small animals. However, calibrating two-wavelength oximetry to
9 3 arterial OS alone, leads to systematic errors in estimating venous OS (see Section 2.1.3 for more details).

10 4 5.3.2. *Oxygen sensitive nanophosphors and dyes*

11
12 5 The pO₂ within blood can be non-invasively verified by imaging of nanophosphor probes with pO₂-
13 6 dependent optical emission properties. In brief, nanophosphors refer to a class of nanoscale
14 7 phosphorescent biochemical probes that emit light and which are bound to a carrier protein, e.g. serum
15 8 albumin. These nanophosphors typically require ultraviolet or blue excitation, which severely limits the
16 9 depth to which they can be imaged within tissue, and which can induce photo-toxicity and tissue auto-
17 10 fluorescence.[133] Additionally, for robust measurement, these nanophosphors require complex
18 11 phosphorescence lifetime imaging equipment. The combination of these factors mean that
19 12 nanophosphor oxygen probes are not widely used for oximetry verification. Dmitriev et al., (2012)
20 13 provide a review of the oxygen-sensitive nanophosphors available, along with associated
21 14 challenges.[133] Shonat et al., (1997) is a good example of verifying MSI oximetry with
22 15 nanophosphors.[65]

23 16 5.3.3. *Physiological interventions that alter oxygen saturation*

24
25 17 Physiological interventions such as systemic hyperoxia, systemic hypoxia, oxygen diffusion, and retinal
26 18 flicker light stimulation enable researchers to induce artificial changes in OS, distinct from physiological
27 19 norms. This enables researchers to verify oximetry capability and test physiological responses to
28 20 stimuli.[6,7,134]

29
30 21 In hyperoxia interventions, excess oxygen is administered to a subject, increasing systemic OS. Arterial
31 22 OS is increased from ~95-97% to 100%, and venous OS increases by a larger margin. Temporary
32 23 hyperoxia is thought to be a safer intervention than temporary hypoxia for subjects with cardiovascular
33 24 impairment, although long-term hyperoxia itself can be damaging.[1] A particularly effective use of a
34 25 temporary hyperoxia intervention was by Kristjansdottir et al., (2013). Their study used hyperoxia to
35 26 demonstrate that choroidal vessels, even veins, are normally highly oxygenated.[14] Without a
36 27 hyperoxia intervention, this insight would not have been possible.[6]

37
38 28 In hypoxia interventions, air with reduced oxygen content is administered to a subject, decreasing both
39 29 arterial and venous OS. Hypoxia is often associated with autoregulation vessel dilation that increases
40 30 flow rate to maintain oxygen consumption.[28] Hypoxia interventions have led to insights that would
41 31 otherwise not be possible, for example, MacKenzie et al., (2016)[15] utilised a hypoxia intervention to
42 32 decrease OS and consequently observed rapid oxygen diffusion from air into bulbar conjunctival
43 33 microvasculature.[15]

44
45 34 Deliberate introduction of oxygen diffusion itself has recently emerged as a new intervention technique
46 35 for oximetry. MacKenzie et al., (2016) utilised eyelid closure to control oxygen diffusion to bulbar
47 36 conjunctival vessels,[135] and van der Putten et al., (2017) surgically exposed blood vessels to air to
48 37 increase OS via diffusion; they blocked diffusion by using oxygen-impermeable plastic film. This
49 38 control of diffusion helped van der Putten et al. verify the oximetry measurement capability of their
50 39 system, and confirmed low initial OS in the blood vessels studied.[10]

51
52 40 In the retinal oximetry studies, flickering light illumination can be used to alter the metabolic demand
53 41 of retinal tissue, and thus change uptake of oxygen by blood, altering OS. Unlike hyperoxia and hypoxia,
54 42 flicker light stimulation does not change systemic OS.[6]

55 43 6. Multispectral oximetry imaging modalities

1 6.1. Time-sequential multispectral imaging

2 Conventional broadband imaging systems (e.g. retinal fundus cameras, microscopes, and endoscopes)
3 can be adapted for MSI by spectrally filtering light prior to detection. There are two basic approaches
4 to MSI oximetry: time-sequential MSI and snapshot MSI.

5 In time-sequential imaging, images at various wavebands are acquired sequentially by switching spectral
6 filters in either the illumination or detection path. Time-sequential filtering technologies include
7 mechanically switched bandpass interference filters, liquid crystal tunable filters (LCTFs), and acousto-
8 optical tunable filters (AOTFs) (see Table 2 for a comparison of these technologies).[136] In addition,
9 laser-based imaging techniques such as scanning laser ophthalmoscopes and photoacoustic techniques
10 rely on time-sequential switching of laser illumination for spectral discrimination.

11 Time-sequential MSI are poorly suited for observation of rapid biological processes which occur in the
12 timescale of milliseconds (e.g. oxygen diffusion). For observing such rapid events, snapshot MSI is
13 preferable.[59]

14
15 **Table 2.** Comparison of electronically switchable optical filter technologies.

16 Filter type	17 Technology type	18 Switching time	19 Spectral Bandwidth	20 Filter operation area and limitations
21 LCTFs	22 Layered liquid crystal filters.	23 ~50 ms	24 ~ 10 nm.	25 Large beam area (e.g. a 25 mm diameter aperture); polarization dependent filtering.[136]
26 AOTFs	27 Radio-frequency acoustic pressure wave modulated crystal transmission filter.	28 ~ 25 μ s	29 ~ 2 nm.	30 Small beam area (e.g. a diameter of a few mm); requires well collimated light.[136]
31 Bandpass filters	32 Filters on a motor-controlled switching mount.	33 ~1 s	34 Typically ~ 10 nm, but highly variable.	35 Large beam area (e.g. 25 mm diameter aperture).

36 6.2. Snapshot multispectral imaging

37 Snapshot MSI technologies enable simultaneous acquisition of images at multiple spectral wavebands
38 reducing oximetry artefacts,[59] and providing sub-second temporal resolution.[5]^{§§} A variety of
39 snapshot MSI imaging systems have been produced,[137–141] but only two approaches have found
40 substantial usage in oximetry: beam-splitter multiplexing and the Image Replicating Imaging
41 Spectrometer (IRIS).

42 Beam splitter multiplexing is the simplest form of MSI and has been incorporated into several retinal
43 oximetry systems.[16,39,40] In such systems, a broadband image is split into two or more paths by one
44 or more beam splitters, producing a cascade of images which can be individually spectrally filtered.

45 ^{§§}NB: an alternative MSI approach is to scan a point or line across a field of view, acquiring a spectral dataset
46 via a spectrometer of the point “in a hyperspectral snapshot”, i.e. the reflectance spectrum from that single
47 point.[38,160] However, this approach doesn’t enable image co-registration to account to subject motion, and
48 hasn’t been widely applied for MSI oximetry.

1
2
3
4
5
6
7 1 However, this approach becomes increasingly optically inefficient with the addition of more beam
8 2 splitters.[59]

9
10 3 The IRIS operates by employing a combination of wave plates and Wollaston prisms to spectrally de-
11 4 multiplex a broadband image in multiple images of distinct wavebands. IRIS systems can be tailored for
12 5 specific applications, including oximetry.[142–144] IRIS has been utilized for measuring rapid oxygen
13 6 release from red blood cells as well as observing fast oxygen diffusion into blood vessels.[5,15,28]

14 15 7 *6.3. Scanning laser ophthalmoscopes*

16
17 8 Scanning laser ophthalmoscopes (SLOs) utilize laser raster scanning to image the retinal reflectance for
18 9 MSI oximetry. Compared to conventional retinal fundus cameras, SLOs can provide advantages in
19 10 spatial resolution, contrast, and imaging field-of-view on the retina. Adaptive optics MSI SLOs have
20 11 been developed to compensate for involuntary eye movement and thus enable imaging of the small
21 12 retinal vessels.[145] Additionally, SLOs can be used in situations where retinal oximetry with a
22 13 multispectral fundus camera would be challenging, such as imaging the retina of infants.[146] However,
23 14 oximetry with MSI SLOs is fundamentally limited by the laser wavelengths available, resulting in sub-
24 15 optimal wavelength combinations for oximetry.[147]

25 26 16 *6.4. Photoacoustic imaging*

27 17
28 18 Since the mid-2000s, photoacoustic imaging techniques^{***} have emerged as a powerful family of MSI
29 19 imaging technologies that combine the advantages of optical absorbance contrast with the advantages
30 20 of ultrasonic detection. Due to this unique combination of properties, photoacoustic techniques can
31 21 provide deep-tissue maps of blood OS without the surrounding tissue. In photoacoustic techniques, a
32 22 high intensity laser pulse (< 10 ns duration) is incident upon blood. This pulse is absorbed, and the blood
33 23 heats up, resulting in rapid expansion and contraction of the blood. This expansion and contraction
34 24 generates ultrasonic pressure waves, which are detected by one or more ultrasound transceivers. The
35 25 amplitude of ultrasound generated by the blood is directly proportional to how much light was absorbed
36 26 by the blood at the illuminating wavelength. Thus, the ratio of ultrasound amplitudes at two or more
37 27 wavelengths can then be related to OS.

38 28 Broadly speaking, there are two variants of photoacoustic imaging: Photoacoustic Tomography (PAT),
39 29 and Photoacoustic Microscopy (PAM), which offer different capabilities in terms of tissue depth
40 30 penetration and spatial resolution.

41 31 In PAT, tissue is diffusely illuminated with a laser pulse, and the resulting ultrasound signal is detected
42 32 and reconstructed by computational back-projection algorithms means to form a 3D optical absorption
43 33 distribution. When imaged at multiple wavelengths, this absorption can then be related to OS in a manner
44 34 similar to conventional oximetry theory (e.g. two-wavelength oximetry). PAT can image blood vessels
45 35 embedded within several centimeters of tissue with a spatial resolution of ~ 10 – 100 μm . [148] Due to
46 36 this capability, PAT is particularly advantageous for deep tissue applications such as whole body small
47 37 animal imaging, brain imaging, and tumor imaging.

48 38 PAM provides higher spatial resolution, but at the expense of imaging depth. In PAM, an image is built
49 39 up by raster scanning a dual-focused optical beam and ultrasound detector across a target. The spatial
50 40 resolution of PAM is determined by the convolution of the PSF of optical spot and ultrasound detector;
51 41 therefore, higher resolution images require higher frequency ultrasound detectors, which greatly reduces
52 42 depth penetration through tissue. Lateral spatial resolution of ~1 μm has been achieved with PAM,
53 43 limited to a depth of ~ 100 μm in tissue.[149,150]

54
55
56
57
58 *** also known as optoacoustic imaging.
59
60

1
2
3
4
5
6
7 1 Despite the impressive capabilities of PAT and PAM, these techniques require complex and expensive
8 2 equipment, acoustically-coupled detection, and intense laser illumination. This makes photoacoustic
9 3 techniques unsuitable for retinal imaging in humans. Further, increasing the temporal resolution of
10 4 photoacoustic techniques is highly challenging.[151] These drawbacks present a considerable barrier of
11 5 entry for new researchers to the field. Consequently, photoacoustic techniques are very powerful, but
12 6 are not yet as widely applied to oximetry as time-sequential or snapshot MSI techniques.

13 14 7 6.5. Spectroscopic Optical Coherence Tomography 15 8

16 9 Spectroscopic Optical Coherence Tomography (S-OCT) is a variant of Optical Coherence Tomography
17 10 (OCT) where the spectral absorbance of blood is inferred from the light back-scattered from blood
18 11 vessels. S-OCT is a point scanning technique, which is spectrally snapshot, but spatially time-sequential
19 12 because the image is built-up from a raster-scanned spot. S-OCT enables 3D maps of OS combined with
20 13 3D mapping of tissue structure. This capability can be used to create 3D maps of tissue features such as
21 14 blood vessel wall thickness,[152] however, all OCT techniques suffer from shadowing from overlying
22 15 tissue and blood vessels. S-OCT has been in development since the mid-2000s and has mainly been
23 16 applied to retinal and brain imaging in animals due to illumination intensity limitations.[153] However,
24 17 S-OCT oximetry in humans was recently demonstrated for the first time: an important and highly
25 18 promising milestone.[42,154]

26 27 19 6.6. Dual-wavelength photothermal optical coherence tomography 28 20

29 20 Dual-Wavelength Photothermal Optical Coherence Tomography (DWPT-OCT), like photoacoustic
30 21 techniques, is based upon heating of blood by light. In DWPT-OCT, light incident upon a blood vessel
31 22 is absorbed by blood, and heats the blood, producing small thermal perturbations (in the order of
32 23 nanometers) proportional to the absorption coefficient of blood, and thus proportional to OS. The very
33 24 small thermal perturbations are then measured by phase-sensitive optical coherence tomography.[155]
34 25 However, to-date DWPT-OCT has been only utilized for oximetry in phantoms and the brain of
35 26 anesthetized mice.[156–158]

36 37 27 7. Summary and Conclusions 38 28

39 28 The tutorial article is designed to serve as a broad introduction to MSI oximetry, whilst still also
40 29 providing detailed content for the more experienced researcher. This article covers the optical theory of
41 30 MSI oximetry, discusses the various MSI oximetry imaging modalities, and describes the many
42 31 challenges encountered when applying MSI oximetry to *in vivo* application.

43 32 For decades, two-wavelength oximetry has been the most widely applied oximetry imaging technique.
44 33 However, multispectral oximetry algorithms techniques have demonstrated considerable promise for the
45 34 myriad and diverse applications where reliable reference OS values are not yet known, pushing the
46 35 boundaries of the field of oximetry. Nevertheless, calibration and verification of all oximetry techniques
47 36 remains a fundamental challenge.

48 37 Imaging modalities for MSI oximetry are rapidly progressing, with several powerful new imaging
49 38 modalities emerging and providing capabilities beyond standard imaging techniques. Snapshot MSI
50 39 technology provides sub-second oximetry capability, providing the ability to observed rapid biological
51 40 processes such as microvascular oxygen diffusion and oxygen release from RBCs. Photoacoustic and
52 41 endoscopic techniques provide deep-tissue oximetry measurement capability, particularly useful in
53 42 applications such as the study of tumour development and rheumatoid arthritis. S-OCT is maturing as a
54 43 viable technique for combined retinal oximetry and retinal tissue structure mapping in the human eye.
55 44 Further, access to powerful computational processing techniques has enabled automatic oximetry
56 45 analysis in a clinical setting.

1
2
3
4
5
6
7 1 In addition to developments of MSI oximetry techniques, new OS-altering physiological interventions,
8 2 have emerged. These interventions, such as temporary hyperoxia, temporary hypoxia, controlled oxygen
9 3 diffusion, and retinal flicker-light stimulation, have proven to be a powerful tool for researchers to assess
10 4 oximetry capability, and explore physiological norms and responses.

11
12 5 Historically, advances in oximetry technology have led to new insights into physiological norms and
13 6 disease development. Given the recent pace of developments in the field of MSI oximetry, it is not
14 7 unreasonable to expect further developments in the understanding of physiology and disease in the
15 8 future.

16
17
18
19
20
21
22
23
24
25
26
27
28
29
30
31
32
33
34
35
36
37
38
39
40
41
42
43
44
45
46
47
48
49
50
51
52
53
54
55
56
57
58
59
60

Accepted Manuscript

1
2
3
4
5
6
7 1 8. References

- 8
9 2 [1] Saugstad O D 2006 Oxygen and retinopathy of prematurity. *J. Perinatol.* **26** S46–50
- 10
11 3 [2] Hardarson S H, Elfarsson A, Agnarsson B A and Stefansson E 2013 Retinal oximetry in
12 4 central retinal artery occlusion *Acta Ophthalmol.* **91** 189–90
- 13
14 5 [3] Sorg B S, Moeller B J, Donovan O, Cao Y and Dewhirst M W 2005 Hyperspectral imaging of
15 6 hemoglobin saturation in tumor microvasculature and tumor hypoxia development *J. Biomed.*
16 7 *Opt.* **10** 44004
- 17
18 8 [4] Sorg B S, Hardee M E, Agarwal N, Moeller B J and Dewhirst M W 2008 Spectral imaging
19 9 facilitates visualization and measurements of unstable and abnormal microvascular oxygen
20 10 transport in tumors. *J. Biomed. Opt.* **13** 14026
- 21
22 11 [5] Fernandez Ramos J, Brewer L R, Gorman A and Harvey A R 2014 Video-rate multispectral
23 12 imaging: application to microscopy and macroscopy *Classical Optics 2014, OSA Technical*
24 13 *Digest* (Washington, D.C.: Optical Society of America)
- 25
26 14 [6] MacKenzie L E, Harvey A R and McNaught A I 2017 Spectroscopic oximetry in the eye: a
27 15 review *Expert Rev. Ophthalmol.* 1–12
- 28
29 16 [7] van der Putten M A, MacKenzie L E, Davies A L, Fernandez-Ramos J, Desai R A, Smith K J
30 17 and Harvey A R 2017 A multispectral microscope for in vivo oximetry of rat dorsal spinal cord
31 18 vasculature *Physiol. Meas.* **38** 205–18
- 32
33 19 [8] Deng Z, Wang Z, Yang X, Luo Q and Gong H 2012 In vivo imaging of hemodynamics and
34 20 oxygen metabolism in acute focal cerebral ischemic rats with laser speckle imaging and
35 21 functional photoacoustic microscopy. *J. Biomed. Opt.* **17** 081415–1
- 36
37 22 [9] van der Putten M A, Brewer J M and Harvey A R 2017 Minimally invasive optical biopsy for
38 23 oximetry *Proc. SPIE 10040, Endosc. Microsc. XII, 1004009*
- 39
40 24 [10] van der Putten M A, Brewer J M and Harvey A R 2017 Multispectral oximetry of murine
41 25 tendon microvasculature with inflammation *Biomed. Opt. Express* **8** 2896
- 42
43 26 [11] Clancy N T, Arya S, Stoyanov D, Singh M, Hanna G B and Elson D S 2015 Intraoperative
44 27 measurement of bowel oxygen saturation using a multispectral imaging laparoscope. *Biomed.*
45 28 *Opt. Express* **6** 4179–90
- 46
47 29 [12] Townsend D, D'Aiuto F and Deanfield J 2015 In Vivo Capillary Loop Hemoglobin
48 30 Spectroscopy in Labial, Sublingual, and Periodontal Tissues *Microcirculation* **22** 475–84
- 49
50 31 [13] Chin M S, Freniere B B, Lo Y-C, Saleeby J H, Baker S P, Strom H M, Ignatz R A, Lalikos J F
51 32 and Fitzgerald T J 2012 Hyperspectral imaging for early detection of oxygenation and
52 33 perfusion changes in irradiated skin. *J. Biomed. Opt.* **17** 26010
- 53
54 34 [14] Kristjansdottir J V, Hardarson S H, Harvey A R, Olafsdottir O B, Eliasdottir T S and Stef E
55 35 2013 Choroidal oximetry with a noninvasive spectrophotometric oximeter *Invest. Ophthalmol.*
56 36 *Vis. Sci.* **54** 3234–9
- 57
58 37 [15] MacKenzie L E, Choudhary T R, McNaught A I and Harvey A R 2016 In vivo oximetry of
59 38 human bulbar conjunctival and episcleral microvasculature using snapshot multispectral

- 1
2
3
4
5
6
7 1 imaging *Exp. Eye Res.* **149** 48–58
- 8
9 2 [16] Tiedeman J S, Kirk S E, Srinivas S and Beach J M 1998 Retinal oxygen consumption during
10 3 hyperglycemia in patients with diabetes without retinopathy *Ophthalmology* **105** 31–6
- 11
12 4 [17] Hammer M, Vilser W, Riemer T, Mandacka A, Schweitzer D, Kühn U, Dawczynski J, Liemt
13 5 F and Strobel J 2009 Diabetic patients with retinopathy show increased retinal venous oxygen
14 6 saturation. *Graefes Arch. Clin. Exp. Ophthalmol.* **247** 1025–30
- 15
16 7 [18] Olafsdottir O B, Hardarson S H, Gottfredsdottir M S, Harris A and Stefánsson E 2011 Retinal
17 8 oximetry in primary open-angle glaucoma. *Invest. Ophthalmol. Vis. Sci.* **52** 6409–13
- 18
19 9 [19] Mordant D J, Al-Abboud I, Muyo G, Gorman A, Harvey A R and McNaught A I 2014
20 10 Oxygen saturation measurements of the retinal vasculature in treated asymmetrical primary
21 11 open-angle glaucoma using hyperspectral imaging. *Eye* **28** 1190–200
- 22
23 12 [20] Boeckaert J, Vandewalle E and Stalmans I 2012 Oximetry: recent insights into retinal
24 13 vasopathies and glaucoma. *Bull. Soc. Belge Ophthalmol.* 75–83
- 25
26 14 [21] Yudovsky D, Nouvong A, Schomacker K and Pilon L 2011 Assessing diabetic foot ulcer
27 15 development risk with hyperspectral tissue oximetry. *J. Biomed. Opt.* **16** 26009
- 28
29 16 [22] Tomaszewski M R, Gonzalez I Q, O'Connor J P B, Abeyakoon O, Parker G J M, Williams K
30 17 J, Gilbert F J and Bohndiek S E 2017 Oxygen enhanced Optoacoustic Tomography (OE-OT)
31 18 reveals vascular dynamics in murine models of prostate cancer *Theranostics* **7** 2900–13
- 32
33 19 [23] Stefansson E, Olafsdottir O B, Einarsdottir A B, Scheving T, Eysteinnsson T, Vehmeijer W,
34 20 Vandewalle E, Bek T and Hardarson S H 2017 Retinal Oximetry Discovers Novel Biomarkers
35 21 in Retinal and Brain Diseases *Investig. Ophthalmol. Vis. Sci.* **58** 227–33
- 36
37 22 [24] Beach J 2014 Pathway to retinal oximetry. *Transl Vis Sci Technol* **3** 1–9
- 38
39 23 [25] Germann W J and Stanfield C L 2005 The cardiovascular system: blood *Principles of Human*
40 24 *Physiology* (Pearson Custom Publishing) pp 496–515
- 41
42 25 [26] Marengo-Rowe A J 2006 Structure-function relations of human hemoglobins *Baylor Univ.*
43 26 *Med. Cent. Proc.* **19** 239–45
- 44
45 27 [27] Germann W J and Stanfield C L 2005 The respiratory system: gas exchange and regulation of
46 28 breathing *Principles of Human Physiology* (Pearson Custom Publishing) pp 516–77
- 47
48 29 [28] Choudhary T R, Ball D, Fernandez Ramos J, McNaught A I and Harvey A R 2013 Assessment
49 30 of acute mild hypoxia on retinal oxygen saturation using snapshot retinal oximetry. *Invest.*
50 31 *Ophthalmol. Vis. Sci.* **54** 38–43
- 51
52 32 [29] Hammer M, Vilser W, Riemer T and Schweitzer D 2008 Retinal vessel oximetry-calibration,
53 33 compensation for vessel diameter and fundus pigmentation, and reproducibility *J. Biomed. Opt.*
54 34 **13** 1–7
- 55
56 35 [30] Prahl S 1999 Optical absorption of hemoglobin *Oregon Med. Laser Cent.*
- 57
58 36 [31] Hickam J B, Sieker H O and Frayser R 1959 Studies of retinal circulation and A-V oxygen
59 37 difference in man. *Trans. Am. Clin. Climatol. Assoc.* **71** 34–44

- 1
2
3
4
5
6
7 1 [32] Hickam J B, Frayser R and Ross J C 1963 A study of retinal venous blood oxygen saturation
8 2 in human subjects by photographic means *Circulation* **27** 375–85
- 9
10 3 [33] Hickam J B and Frayser R 1966 Studies of the retinal circulation in man. Observations on
11 4 vessel diameter, arteriovenous oxygen difference, and mean circulation time *Circulation*
12 5 **XXXIII** 302–16
- 13
14 6 [34] Aoyagi T 2003 Pulse oximetry: its invention, theory, and future *J. Anesth.* **17** 259–66
- 15
16 7 [35] Pittman R and Duling B 1975 A new method for the measurement of percent oxyhemoglobin
17 8 *J. Appl. Physiol.* **38**
- 18
19 9 [36] Delori F C 1988 Noninvasive technique for oximetry of blood in retinal vessels. *Appl. Opt.* **27**
20 10 1113–25
- 21
22 11 [37] Delori F C 1994 Spectrophotometer for noninvasive measurement of intrinsic fluorescence
23 12 and reflectance of the ocular fundus. *Appl. Opt.* **33** 7439–52
- 24
25 13 [38] Hammer M and Schweitzer D 2002 Quantitative reflection spectroscopy at the human ocular
26 14 fundus. *Phys. Med. Biol.* **47** 179–91
- 27
28 15 [39] Beach J M, Schwenzler K J, Srinivas S, Kim D and Tiedeman J S 1999 Oximetry of retinal
29 16 vessels by dual-wavelength imaging: calibration and influence of pigmentation *J. Appl.*
30 17 *Physiol.* **86** 748–58
- 31
32 18 [40] Hardarson S H, Harris A, Karlsson R A, Halldorsson G H, Kagemann L, Rechtman E, Zoega
33 19 G M, Eysteinnsson T, Benediktsson J A, Thorsteinsson A, Jensen P K, Beach J and Stefánsson E
34 20 2006 Automatic retinal oximetry. *Invest. Ophthalmol. Vis. Sci.* **47** 5011–6
- 35
36 21 [41] Mehrmohammadi M, Yoon S J, Yeager D and Emelianov S Y 2013 Photoacoustic imaging for
37 22 cancer detection and staging *Curr. Mol. Imaging* **2** 89–105
- 38
39 23 [42] Chen S, Shu X, Nesper P L, Liu W, Fawzi A A and Zhang H F 2017 Retinal oximetry in
40 24 humans using visible-light optical coherence tomography [Invited] *Biomed. Opt. Express* **8**
41 25 1415–29
- 42
43 26 [43] van Assendelft O W. 1970 Spectrophotometry of haemoglobin derivatives *Van Gorcum*
- 44
45 27 [44] Smith M H 1999 Optimum wavelength combinations for retinal vessel oximetry. *Appl. Opt.* **38**
46 28 258–67
- 47
48 29 [45] LeBlanc S E, Atanya M, Burns K and Munger R 2011 Quantitative impact of small angle
49 30 forward scatter on whole blood oximetry using a Beer-Lambert absorbance model. *Analyst* **136**
50 31 1637–43
- 51
52 32 [46] Briley-Saebo K and Bjornerud A 2000 Accurate de-oxygenation of ex vivo whole blood using
53 33 sodium dithionite. *Proc. Intl. Soc. Mag. Reson. Med* **8** 2025
- 54
55 34 [47] Allen J 2007 Photoplethysmography and its application in clinical physiological measurement
56 35 *Physiol. Meas.* **28**
- 57
58 36 [48] Hanning C D, Alexander-Williams and Jm 1995 Pulse oximetry: a practical review *Br. Med. J.*
59
60

- 1
2
3
4
5
6
7 1 311 367–70
- 8
9 2 [49] Avidan A and Levin P D 2011 Pulse oximetry *N. Engl. J. Med.* **365** 184–5
- 10
11 3 [50] Taylor M . and Whitwam J G 1988 The accuracy of pulse oximeters *Anesthesia* **43** 229–32
- 12
13 4 [51] Haynes J M 2007 The ear as an alternative site for a pulse oximeter finger clip sensor *Respir. Care* **52** 727–9
- 14
15
16 6 [52] Papanas N, Kakagia D, Papatheodorou K, Papazoglou D, Alexandridou M, Pagkalos a, Karadimas E J and Maltezos E 2010 Lanarkshire Oximetry Index as a diagnostic tool for peripheral arterial disease in type 2 diabetes: a pilot study. *Angiology* **61** 388–91
- 17
18 8
19
20 9 [53] Das J, Aggarwal A and Aggarwal N K 2010 Pulse oximeter accuracy and precision at five different sensor locations in infants and children with cyanotic heart disease *Indian J. Anaesth.* **54** 531–4
- 21
22 10
23 11
24 12 [54] Chen H W, Weng L C, Wang T M and Ng K F 2014 Potential use of pulse oximetry for the diagnosis of testicular torsion *JAMA Pediatr* **168** 578–9
- 25
26 13
27 14 [55] Comber J T and Lopez B L 1996 Evaluation of pulse oximetry in sickle cell anemia patients presenting to the emergency department in acute vasoocclusive crisis. *Am. J. Emerg. Med.* **14** 16–8
- 28
29 15
30 16
31 17 [56] Smith M H, Denninghoff K R, Lompadro A and Hillman L W 2000 Effect of multiple light paths on retinal vessel oximetry. *Appl. Opt.* **39** 1183–93
- 32
33 18
34 19 [57] Faber D, Aalders M, Mik E, Hooper B, van Gemert M and van Leeuwen T 2004 Oxygen saturation-dependent absorption and scattering of blood *Phys. Rev. Lett.* **93** 2–5
- 35
36 20
37 21 [58] Rodmell P I, Crowe J A, Gorman A, Harvey A R, Muyo G, Mordant D J, McNaught A I and Morgan S P 2014 Light path-length distributions within the retina. *J. Biomed. Opt.* **19** 36008
- 38
39 22
40 23 [59] Hendargo H C, Zhao Y, Allenby T and Palmer G M 2015 Snap-shot multispectral imaging of vascular dynamics in a mouse window-chamber model *Opt. Lett.* **40** 3292–3295
- 41
42 24
43 25 [60] Mordant D J, Al-Abboud I, Muyo G, Gorman A, Sallam A, Ritchie P, Harvey a R and McNaught a I 2011 Spectral imaging of the retina. *Eye* **25** 309–20
- 44
45 26
46 27 [61] Alabboud I, Muyo G, Gorman A, Mordant D, McNaught A, Petres C, Petillot Y R and Harvey A R 2007 New spectral imaging techniques for blood oximetry in the retina ed C D Depeursinge *Proc. SPIE 6631, Nov. Opt. Instrum. Biomed. Appl. III* **6631**
- 47
48 28
49 29
50 30 [62] Denninghoff K R and Smith M H 2000 Optical model of the blood in large retinal vessels. *J. Biomed. Opt.* **5** 371–4
- 51
52 31
53 32 [63] Drewes J, Smith M, Hiliman L, Jonathan J D, Matthew H S, Kurt R D and Lloyd W H 1999 Instrument for the measurement of retinal vessel oxygen saturation *BiOS'99 Int. Biomed. Opt. Symp. Int. Soc. Opt. Photonics* **3591** 114–20
- 54
55 33
56 34
57 35 [64] Schweitzer D, Hammer M, Kraft J, Thamm E, Königsdörffer E and Strobel J 1999 In vivo measurement of the oxygen saturation of retinal vessels in healthy volunteers. *IEEE Trans.*
- 58
59 36
60

- 1
2
3
4
5
6
7 1 *Biomed. Eng.* **46** 1454–65
- 8
9 2 [65] Shonat R D and Wachman S 1997 Near-simultaneous hemoglobin saturation and oxygen
10 3 tension maps in mouse brain using an AOTF microscope *Biophys. J.* **73** 1223–31
- 11
12 4 [66] Zijlstra W G, Buursma A, Falke H E and Catsburg J F 1994 Spectrophotometry of
13 5 hemoglobin: absorption spectra of rat oxyhemoglobin, deoxyhemoglobin, carboxyhemoglobin,
14 6 and methemoglobin *Comp. Biochem. Physiol.* **107** 161–6
- 15
16 7 [67] Zijlstra W G and Buursma A 1997 Spectrophotometry of hemoglobin: absorption spectra of
17 8 bovine oxyhemoglobin, deoxyhemoglobin, carboxyhemoglobin, and methemoglobin *Comp.*
18 9 *Biochem. Physiol.* **118** 743–9
- 19
20 10 [68] Zijlstra W, Buursma A and Meeuwse-van der Roest W 1991 Absorption Spectra of Human
21 11 Fetal and Adult Oxyhemoglobin, De-Oxyhemoglobin, and Methemoglobin *Clin. Chem.* **37**
22 12 1633–8
- 23
24 13 [69] Brunori M and Vallone B 2006 A globin for the brain *Faseb J* **20** 2192–7
- 25
26 14 [70] Lisenko S A, Firago V A, Kugeiko M M and Kubarko A I 2016 Determination of Structural
27 15 and Morphological Parameters of Human Bulbar Conjunctiva from Optical Diffuse
28 16 Reflectance Spectra *J. Appl. Spectrosc.* **83** 617–26
- 29
30 17 [71] MacKenzie L E, Choudhary T R, McNaught A I and Harvery A R 2017 Comment on the
31 18 influence of episcleral blood vessels in diffuse reflectance spectroscopy measurements of the
32 19 bulbar conjunctiva *J. Appl. Spectrosc.* **84** 174–85
- 33
34 20 [72] Lisenko S A, Firago V A, Kugeiko M M and Kubarko A I 2017 Response from Authors of
35 21 “Determination of Structural and Morphological Parameters of Human Bulbar Conjunctiva
36 22 from Optical Diffuse Reflectance Spectra,” *J. Appl. Spectrosc.*, 83, No. 4, 617–626 (2016) to
37 23 L. E. MacKenzie, T. R. Choudhary, A. I. McNaught, a *J. Appl. Spectrosc.* **84** 204–5
- 38
39 24 [73] Castaldo A M, Ercolini P, Forino F, Basevi A, Vrenna L, Castaldo P, D’Ambrosio V and
40 25 Castaldo A 1994 Plasma myoglobin in the early diagnosis of acute myocardial infarction *Eur J*
41 26 *Clin Chem Clin Biochem* **32** 349–53
- 42
43 27 [74] Brancaccio P, Lippi G and Maffulli N 2010 Biochemical markers of muscular damage *Clin.*
44 28 *Chem. Lab. Med.* **48** 757–67
- 45
46 29 [75] Bowen J 1948 The absorption spectra and extinction coefficients of myoglobin *J. Biol. Chem.*
47 30 **179** 235–46
- 48
49 31 [76] Meinke M, Müller G, Helfmann J and Friebel M 2007 Optical properties of platelets and
50 32 blood plasma and their influence on the optical behavior of whole blood in the visible to near
51 33 infrared wavelength range *J. Biomed. Opt.* **12** 14024
- 52
53 34 [77] Meinke M, Müller G, Helfmann J and Friebel M 2015 Optical properties of platelets and blood
54 35 plasma and their influence on the optical behavior of whole blood in the visible to near infrared
55 36 wavelength range. *J. Biomed. Opt.* **12** 14024
- 56
57
58 37 [78] Wolfbeis O S and Leiner M 1985 Mapping of the total fluorescence of human blood serum as
59 38 a new method for its characterization *Anal. Chim. Acta* **167** 203–15
- 60

- 1
2
3
4
5
6
7 1 [79] Jacques S L 2013 Optical properties of biological tissues: a review. *Phys. Med. Biol.* **58** R37-
8 2 61
- 9
10 3 [80] Franssen L, Coppens J E and van den Berg T J T P 2008 Grading of iris color with an
11 4 extended photographic reference set *J. Optom.* **1** 36–40
- 12
13 5 [81] Bashkatov A N, Genina E A, Kochubey V I and Tuchin V V 2005 Optical properties of human
14 6 skin, subcutaneous and mucous tissues in the wavelength range from 400 to 2000 nm *J. Phys.*
15 7 *D. Appl. Phys.* **38** 2543–55
- 16
17 8 [82] Van Gemert M J C, Jacques S L, Sterenborg H J C M and Star W M 1989 Skin optics *IEEE*
18 9 *Trans. Biomed. Eng.* **36** 1146–54
- 19
20 10 [83] Bashkatov A N, Genina E a. and Tuchin V V. 2011 Optical properties of skin, subcutaneous,
21 11 and muscle tissues: a review *J. Innov. Opt. Health Sci.* **4** 9–38
- 22
23 12 [84] Sardar D K, Yow R M, Tsin A T C and Sardar R 2005 Optical scattering, absorption, and
24 13 polarization of healthy and neovascularized human retinal tissues. *J. Biomed. Opt.* **10** 51501
- 25
26 14 [85] Sardar D K, Swanland G-Y, Yow R M, Thomas R J and Tsin A T C 2007 Optical properties of
27 15 ocular tissues in the near infrared region. *Lasers Med. Sci.* **22** 46–52
- 28
29 16 [86] Bashkatov A N, Genina E A, Kochubey V I and Tuchin V V. 2010 Optical properties of
30 17 human sclera in spectral range 370-2500 nm *Opt. Spectrosc.* **109** 197–204
- 31
32 18 [87] Friebel M, Roggan A, Müller G and Meinke M 2006 Determination of optical properties of
33 19 human blood in the spectral range 250 to 1100 nm using Monte Carlo simulations with
34 20 hematocrit-dependent effective scattering phase functions. *J. Biomed. Opt.* **11** 34021
- 35
36 21 [88] Tuchin V V, Xu X and Wang R K 2002 Dynamic optical coherence tomography in studies of
37 22 optical clearing, sedimentation, and aggregation of immersed blood. *Appl. Opt.* **41** 258–71
- 38
39 23 [89] Wen X, Mao Z, Han Z, Tuchin V V and Zhu D 2010 In vivo skin optical clearing by glycerol
40 24 solutions: mechanism. *J. Biophotonics* **3** 44–52
- 41
42 25 [90] Ntziachristos V 2010 Going deeper than microscopy: the optical imaging frontier in biology.
43 26 *Nat. Methods* **7** 603–14
- 44
45 27 [91] Jeon M and Kim C 2013 Multimodal Photoacoustic Tomography *IEEE Trans. Multimed.* 975–
46 28 82
- 47
48 29 [92] Peli E and Schwartz B 1987 Enhancement of fundus photographs taken through cataracts.
49 30 *Ophthalmology* **Pt 2** 10–3
- 50
51 31 [93] Patel S R, Hudson C, Flanagan J G and Heitmar R 2013 The effect of simulated cataract light
52 32 scatter on retinal vessel oximetry *Exp. Eye Res.* **116** 185–9
- 53
54 33 [94] Heitmar R and Attardo A 2016 The influence of simulated cataract on retinal vessel oximetry
55 34 measurements *Acta Ophthalmol.* **94** 48–55
- 56
57 35 [95] Baumann B, Rauscher S, Glösmann M, Götzinger E, Pircher M, Fialová S, Gröger M and
58 36 Hitzemberger C K 2014 Peripapillary rat sclera investigated in vivo with polarization-sensitive

- 1
2
3
4
5
6
7 1 optical coherence tomography *Investig. Ophthalmol. Vis. Sci.* **55** 7686–96
- 8
9 2 [96] Knighton R W and Huang X R 2002 Linear birefringence of the central human cornea
10 3 *Investig. Ophthalmol. Vis. Sci.* **43** 82–6
- 11
12 4 [97] Fariza E, O’Day T, Jalkh A E and Medina A 1989 Use of cross-polarized light in anterior
13 5 segment photography. *Arch. Ophthalmol.* **107** 608–10
- 14
15 6 [98] Cense B, Chen T C, Park B H, Pierce M C and De Boer J F 2004 Thickness and birefringence
16 7 of healthy retinal nerve fiber layer tissue measured with polarization-sensitive optical
17 8 coherence tomography *Investig. Ophthalmol. Vis. Sci.* **45** 2606–12
- 18
19 9 [99] Heitmar R and Kalitzeos A A 2015 Reliability of retinal vessel calibre measurements using a
20 10 retinal oximeter *BMC Ophthalmol.* **15** 184
- 21
22 11 [100] MacKenzie L E, Choudhary T R, McNaught A I and Harvey A R 2016 In vivo oximetry of
23 12 human bulbar conjunctival and episcleral microvasculature using snapshot multispectral
24 13 imaging *Exp. Eye Res.* **149** 48–58
- 25
26 14 [101] Yung M, Klufas M A and Sarraf D 2016 Clinical applications of fundus autofluorescence in
27 15 retinal disease *Int. J. Retin. Vitreol.* **2** 12
- 28
29 16 [102] Friebel M, Helfmann J, Netz U and Meinke M 2009 Influence of oxygen saturation on the
30 17 optical scattering properties of human red blood cells in the spectral range 250 to 2,000 nm. *J.*
31 18 *Biomed. Opt.* **14** 34001
- 32
33 19 [103] Faber D J, van der Meer F J, Aalders M C G and van Leeuwen T G 2006 Hematocrit-
34 20 dependence of the scattering coefficient of blood determined by optical coherence tomography
35 21 *Proc. SPIE 6163, Saratov Fall Meet. 2005 Opt. Technol. Biophys. Med. VII* **6163**
- 36
37 22 [104] Mansouri K, Medeiros F A, Marchase N, Tatham A J, Auerbach D and Weinreb R N 2013
38 23 Assessment of choroidal thickness and volume during the water drinking test by swept-source
39 24 optical coherence tomography *Ophthalmology* **120** 2508–16
- 40
41 25 [105] Klose H J, Volger E, Brechtelsbauer H, Heinich L and Schmid-Schönbein H 1972
42 26 Microrheology and light transmission of blood *Pflügers Arch. - Eur. J. Physiol.* **333** 126–39
- 43
44 27 [106] Blausen.com staff 2014 Medical gallery of Blausen Medical
- 45
46 28 [107] Cimalla P, Walther J, Mittasch M and Koch E 2011 Shear flow-induced optical inhomogeneity
47 29 of blood assessed in vivo and in vitro by spectral domain optical coherence tomography in the
48 30 1.3 μm wavelength range. *J. Biomed. Opt.* **16** 116020
- 49
50 31 [108] Skalak R and Branemark P I 1969 Deformation of red blood cells in capillaries. *Science* **164**
51 32 717–9
- 52
53 33 [109] Salyer D A, Beaudry N, Basavanthappa S, Twietmeyer K, Eskandari M, Denninghoff K R,
54 34 Chipman R a and Park R I 2006 Retinal oximetry using intravitreal illumination. *Curr. Eye*
55 35 *Res.* **31** 617–27
- 56
57
58 36 [110] Rodmell P I, Crowe J A, Gorman A, Harvey A R, Muyo G, Mordant D J, McNaught A I and
59 37 Morgan S P 2014 Light path-length distributions within the retina. *J. Biomed. Opt.* **19** 36008
- 60

- 1
2
3
4
5
6
7 1 [111] Groner W, Winkelman J W, Harris A G, Ince C, Bouma G J, Messmer K and Nadeau R G
8 2 1999 Orthogonal polarization spectral imaging: a new method for study of the
9 3 microcirculation. *Nat. Med.* **5** 1209–13
- 10 4 [112] Hammer M, Leistriz S, Leistriz L and Schweitzer D 2001 Light paths in retinal vessel
11 5 oxymetry. *IEEE Trans. Biomed. Eng.* **48** 592–8
- 12 6 [113] Eliasdottir T S, Bragason D, Hardarson S H, Vacchiano C, Gislason T, Kristjansdottir J V,
13 7 Kristjansdottir G and Stefánsson E 2017 Retinal Oximetry measures systemic hypoxia in
14 8 central nervous system vessels in Chronic Obstructive Pulmonary Disease *PLoS One* **12**
- 15 9 [114] Krogh A 1919 The number and distribution of capillaries in muscles with calculations of the
16 10 oxygen pressure head necessary for supplying the tissue *J. Physiol.* **52** 409–15
- 17 11 [115] Krogh A 1919 The rate of diffusion of gases through animal tissues, with some remarks on the
18 12 coefficient of invasion. *J. Physiol.* **52** 391–408
- 19 13 [116] Krogh A 1919 The supply of oxygen to the tissues and the regulation of the capillary
20 14 circulation *J. Physiol.* **52** 457–474
- 21 15 [117] Sasaki N, Horinouchi H, Ushiyama A and Minamitani H 2012 A New Method for Measuring
22 16 the Oxygen Diffusion Constant and Oxygen Consumption Rate of Arteriolar Walls *Keio J.*
23 17 *Med.* 57–65
- 24 18 [118] Sarkar P K, Pal S, Polley N, Aich R, Adhikari A, Halder A, Chakrabarti S, Chakrabarti P and
25 19 Pal S K 2017 Development and validation of a noncontact spectroscopic device for hemoglobin
26 20 estimation at point-of-care *J. Biomed. Opt.* **22** 55006
- 27 21 [119] Willerslev A, Li X Q, Munch I C and Larsen M 2014 Flow patterns on spectral-domain optical
28 22 coherence tomography reveal flow directions at retinal vessel bifurcations *Acta Ophthalmol.* **92**
29 23 461–4
- 30 24 [120] Weisstein E W 2004 Affine transformation
- 31 25 [121] Cideciyan A V 1995 Registration of ocular fundus images *IEEE Eng. Med. Biol. Mag.* **14** 52–
32 26 8
- 33 27 [122] Can A, Stewart C V., Roysam B and Tanenbaum H L 2002 A feature-based, robust,
34 28 hierarchical algorithm for registering pairs of images of the curved human retina *IEEE Trans.*
35 29 *Pattern Anal. Mach. Intell.* **24** 347–64
- 36 30 [123] Shahidi M, Wanek J, Gaynes B and Wu T 2010 Quantitative assessment of conjunctival
37 31 microvascular circulation of the human eye. *Microvasc. Res.* **79** 109–13
- 38 32 [124] Fischer M J M, Uchida S and Messlinger K 2010 Measurement of meningeal blood vessel
39 33 diameter in vivo with a plug-in for ImageJ *Microvasc. Res.* **80** 258–66
- 40 34 [125] Butler I B, Schoonen M A A and Rickard D T 1994 Removal of dissolved oxygen from water:
41 35 A comparison of four common techniques *Talanta* **41** 211–5
- 42 36 [126] Di Caprio G, Stokes C, Higgins J M and Schonbrun E 2015 Single-cell measurement of red
43 37 blood cell oxygen affinity *Proc. Natl. Acad. Sci.* **112** 9984–9
- 44
45
46
47
48
49
50
51
52
53
54
55
56
57
58
59
60

- 1
2
3
4
5
6
7 1 [127] Partridge M, James S W and Tatam R P 2016 Dissolved oxygen sensing using an optical fibre
8 2 long period grating coated with hemoglobin *J. Light. Technol.* **34** 4506–10
- 9
10 3 [128] Wang J, Ghassemi P, Melchiorri A, Ramella-Roman J, Mathews S a., Coburn J, Sorg B, Chen
11 4 Y and Pfefer J 2015 3D printed biomimetic vascular phantoms for assessment of hyperspectral
12 5 imaging systems *Des. Perform. Valid. Phantoms Used Conjunction with Opt. Meas. Tissue VII,*
13 6 *Proc. SPIE.* **9325**
- 14
15 7 [129] Mordant D J, Al-Abboud I, Muyo G, Gorman A, Sallam A, Rodmell P, Crowe J, Morgan S,
16 8 Ritchie P, Harvey A R and McNaught A I 2011 Validation of human whole blood oximetry,
17 9 using a hyperspectral fundus camera with a model eye. *Invest. Ophthalmol. Vis. Sci.* **52** 2851–9
- 18
19 10 [130] Corcoran A T, Muyo G, van Hemert J I and Harvey A R 2014 Development of a widefield
20 11 phantom eye for retinal optical coherence tomography ed R J Nordstrom, J-P Bouchard and D
21 12 W Allen **894589450F**
- 22
23 13 [131] General Assembly of the World Medical Association. 2014 Declaration of Helsinki World
24 14 Medical Association Declaration of Helsinki *J. Am. Coll. Dent.* **81**
- 25
26 15 [132] Festing S and Wilkinson R 2007 The ethics of animal research *EMBO Rep.* 526–30
- 27
28 16 [133] Dmitriev R I and Papkovsky D B 2012 Optical probes and techniques for O₂ measurement in
29 17 live cells and tissue. *Cell. Mol. Life Sci.* **69** 2025–39
- 30
31 18 [134] Yi J, Liu W, Chen S, Backman V, Sheibani N, Sorenson C M, Fawzi A A, Linsenmeier R A
32 19 and Zhang H F 2015 Visible light optical coherence tomography measures retinal oxygen
33 20 metabolic response to systemic oxygenation *Light Sci. Appl.* **4** e334
- 34
35 21 [135] MacKenzie L E, Choudhary T R, McNaught A I and Harvey A R 2016 In vivo oximetry of
36 22 human bulbar conjunctival and episcleral microvasculature using snapshot multispectral
37 23 imaging *Exp. Eye Res.* **149** 48–58
- 38
39 24 [136] Levenson R 1998 Spectral imaging in biomedicine: A selective overview *Proc. SPIE* **3438**
40 25 300–12
- 41
42 26 [137] Ramella-Roman J C and Mathews S A 2007 Spectroscopic measurements of oxygen saturation
43 27 in the retina *IEEE J. Sel. Top. Quantum Electron.* **13** 1697–703
- 44
45 28 [138] Gao L, Kester R T, Hagen N and Tkaczyk T S 2010 Snapshot Image Mapping Spectrometer
46 29 (IMS) with high sampling density for hyperspectral microscopy. *Opt. Express* **18** 14330–44
- 47
48 30 [139] Gao L, Smith R T and Tkaczyk T S 2012 Snapshot hyperspectral retinal camera with the
49 31 Image Mapping Spectrometer (IMS). *Biomed. Opt. Express* **3** 48–54
- 50
51 32 [140] Ford B K, Volin C E, Murphy S M, Lynch R M and Descour M R 2001 Computed
52 33 tomography-based spectral imaging for fluorescence microscopy *Biophys. J.* **80** 986–93
- 53
54 34 [141] Johnson W R, Wilson D W, Fink W, Humayun M and Bearman G 2007 Snapshot
55 35 hyperspectral imaging in ophthalmology. *J. Biomed. Opt.* **12** 14036
- 56
57 36 [142] Harvey A R, Fletcher-Holmes D W, Kudesia S S and Beggan C 2004 Imaging spectrometry at
58 37 visible and infrared wavelengths using image replication *Proceeding SPIE. Electro-Optical*
- 59
60

- 1
2
3
4
5
6
7 1 *Infrared Syst. Technol. Appl.* **5612** 190–8
- 8
9 2 [143] Harvey A R, Fletcher-Holmes D W, Gorman A, Altenbach K, Arlt J and Read N D 2005
10 3 Spectral imaging in a snapshot *Proc. SPIE. Spectr. Imaging Instrumentation, Appl. Anal. III*
11 4 **5694** 110–9
- 12
13 5 [144] Gorman A, Fletcher-Holmes D W and Harvey A R 2010 Generalization of the Lyot filter and
14 6 its application to snapshot spectral imaging. *Opt. Express* **18** 5602–8
- 15
16 7 [145] Li H, Lu J, Shi G and Zhang Y 2011 Measurement of oxygen saturation in small retinal
17 8 vessels with adaptive optics confocal scanning laser ophthalmoscopy *J. Biomed. Opt.* **16**
- 18
19 9 [146] Vehmeijer W B, Magnusdottir V, Eliasdottir T S, Hardarson S H, Schalijs-Delfos N E and
20 10 Stefánsson E 2016 Retinal Oximetry with Scanning Laser Ophthalmoscope in Infants *PLoS*
21 11 *One* **11** e0148077
- 22
23 12 [147] Kristjansdottir J V, Hardarson S H, Halldorsson G H, Karlsson R A, Eliasdottir T S and
24 13 Stefánsson E 2014 Retinal oximetry with a scanning laser ophthalmoscope *Investig.*
25 14 *Ophthalmology Vis. Sci.* **55** 3120
- 26
27 15 [148] Wang L V and Hu S 2012 Photoacoustic tomography: in vivo imaging from organelles to
28 16 organs. *Science* **335** 1458–62
- 29
30 17 [149] Hu S and Wang L V 2013 Photoacoustic imaging and characterization of the
31 18 microvasculature. *J. Biomed. Opt.* **15** 11101
- 32
33 19 [150] Wang L, Maslov K and Wang L V 2013 Single-cell label-free photoacoustic flowoxigraphy in
34 20 vivo. *Proc. Natl. Acad. Sci. U. S. A.* **2013** 1–6
- 35
36 21 [151] Xiang L, Wang B, Ji L and Jiang H 2013 4-D photoacoustic tomography *Sci. Rep.* **3**
- 37
38 22 [152] Pi S, Camino A, Zhang M, Cepurna W, Liu G, Huang D, Morrison J and Jia Y 2017
39 23 Angiographic and structural imaging using high axial resolution fiber-based visible-light OCT
40 24 *Biomed. Opt. Express* **8** 3127–37
- 41
42 25 [153] Liu W and Zhang H F 2016 Photoacoustic imaging of the eye : a mini review *Biochem.*
43 26 *Pharmacol.*
- 44
45 27 [154] Yi J, Chen S, Shu X, Fawzi A A and Zhang H F 2015 Human retinal imaging using visible-
46 28 light optical coherence tomography guided by scanning laser ophthalmoscopy *Biomed. Opt.*
47 29 *Express* **6** 3701
- 48
49 30 [155] Kuranov R V, Qiu J, McElroy A B, Estrada A, Salvaggio A, Kiel J, Dunn A K, Duong T Q
50 31 and Milner T E 2011 Depth-resolved blood oxygen saturation measurement by dual-
51 32 wavelength photothermal (DWP) optical coherence tomography. *Biomed. Opt. Express* **2** 491–
52 33 504
- 53
54 34 [156] Kuranov R V, Kazmi S, McElroy A B, Kiel J W, Dunn A K, Milner T E and Duong T Q 2011
55 35 In vivo depth-resolved oxygen saturation by Dual-Wavelength Photothermal (DWP) OCT.
56 36 *Opt. Express* **19**
- 57
58 37 [157] Yin B, Kuranov R V, McElroy A B, Kazmi S, Dunn A K, Duong T Q and Milner T E 2013
59 38 Dual-wavelength photothermal optical coherence tomography for imaging microvasculature

- 1
2
3
4
5
6
7 1 blood oxygen saturation. *J. Biomed. Opt.* **18**
- 8
9 2 [158] Yin B, Kuranov R V, Mcelroy A B and Milner T E 2013 Dual-wavelength photothermal
10 3 optical coherence tomography for blood oxygen saturation measurement *Opt. Coherence*
11 4 *Tomogr. Coherence Domain Opt. Methods Biomed.* **8571** 1–7
- 12
13 5 [159] Kienle A, Lilge L, Vitkin I A, Patterson M S, Wilson B C, Hibst R and Steiner R 1996 Why
14 6 do veins appear blue? A new look at an old question *Appl. Opt.* **35** 1151–60
- 15
16 7 [160] Beach J 2002 Spectral reflectance technique for retinal blood oxygen evaluation in humans
17 8 *Proc. 31st Appl. Imag. Pattern Recognit. Work. (AIPR '02)*
- 18
19 9

20
21 10 Acknowledgements

22
23 11 This PhD tutorial stems from a body of knowledge built up over the past decade by various researchers
24 12 in the Imaging Concepts Group, led by Professor Andrew Harvey at the University of Glasgow. Lewis
25 13 MacKenzie's PhD in multispectral imaging oximetry, undertaken between 2012 and 2016, was
26 14 supported by the University of Glasgow Sensors Initiative. Lewis MacKenzie would like to
27 15 acknowledge and thank his PhD supervisors, Professor Andrew Harvey and Dr Ik Siong Heng, for their
28 16 support and knowledge. In addition, he would like to thank colleagues in the Imaging Concepts Group
29 17 at the University of Glasgow, who provided support, expertise, and encouragement during his PhD. In
30 18 particular: Dr Tushar R. Choudhary, Marieke van der Putten, Dr Javier Fernandez Ramos, Dr Laurence
31 19 Brewer, and Dr Ied Al-Abboud. Additional thanks go to various collaborators, including Professor Andy
32 20 I. McNaught, Dr Andrew L. Davies, Dr Roshni A. Desai, Professor Kenneth J. Smith, and Professor
33 21 Christian Delles. Thanks to Cecilie A. Osnes for proof-reading. In addition, we would like to thank the
34 22 anonymous reviewers, particularly reviewer 2, for their helpful comments and prompts. We also
35 23 acknowledge and thank global research community who have worked to advance the field of
36 24 multispectral imaging oximetry since the 1950s.

37
38
39
40
41
42
43
44
45
46
47
48
49
50
51
52
53
54
55
56
57
58
59
60